THE ASTROPHYSICAL JOURNAL, 483:475–495, 1997 July 1
© 1997. The American Astronomical Society. All rights reserved. Printed in U.S.A.

STELLAR SAPPHIRES: THE PROPERTIES AND ORIGINS OF PRESOLAR Al_2O_3 IN METEORITES

LARRY R. NITTLER,[1] CONEL M. O'D. ALEXANDER,[1] XIA GAO, ROBERT M. WALKER, AND ERNST ZINNER
McDonnell Center for the Space Sciences and Physics Department, Washington University, St. Louis, MO 63130
Received 1996 October 7; accepted 1997 January 28

ABSTRACT

Thirty-seven isotopically highly anomalous presolar Al_2O_3 grains and one presolar $MgAl_2O_4$ grain from a separate of the Tieschitz H3.6 ordinary chondrite were identified out of 17,000 isotopically normal refractory oxide grains by an automatic $^{16}O/^{18}O$ low mass resolution ion-imaging mapping technique in the ion microprobe. Eight additional presolar Al_2O_3 grains were found by high mass resolution ion probe measurements of all three stable O isotopes in individual grains, including several that would have been missed by the ion-imaging search. Forty-five of the grains were analyzed for their $^{16}O/^{17}O$ and $^{16}O/^{18}O$ ratios. Twenty-four grains were also analyzed for Al-Mg and 17 of them have large excesses of ^{26}Mg, attributable to the radioactive decay of ^{26}Al. The highly anomalous isotopic composition of the grains is evidence for their presolar, stellar origin.

The 46 oxide grains of this study together with 42 previously identified presolar grains were divided into four groups. These groups most likely comprise grains from distinct types of stellar sources. *Group 1* grains have ^{17}O excesses and moderate ^{18}O depletions, relative to solar, and many of them exhibit ^{26}Mg excesses as well. *Group 2* grains have ^{17}O excesses, large ^{18}O depletions, and high inferred $^{26}Al/^{27}Al$ ratios. *Group 3* grains have solar or higher $^{16}O/^{17}O$ and $^{16}O/^{18}O$ ratios. *Group 4* grains have ^{17}O and ^{18}O enrichments. One Al_2O_3 grain of this study, T54, has an $^{16}O/^{17}O$ ratio of 71, lower than any previously observed, and $^{16}O/^{18}O$ much greater than the solar value.

The O-isotopic compositions of Group 1 and Group 3 grains are consistent with an origin in O-rich red giant stars, which have undergone the first dredge-up. The range of O-isotopic ratios of these groups requires multiple stellar sources of different masses and initial isotopic compositions and is well explained by a combination of Galactic chemical evolution and first dredge-up models. The inferred $^{26}Al/^{27}Al$ ratios of many of these grains indicate that they formed in thermally pulsing asymptotic branch (TP-AGB) stars that had undergone the third dredge-up. Group 2 grains probably formed in low-mass AGB stars as well, and their substantial ^{18}O depletions are the likely result of "extra" mixing (cool bottom processing). The origin of the ^{18}O enrichments in Group 4 grains is unknown, but it might be due to initial compositional differences of the stellar sources or to unusual third dredge-up in low-mass AGB stars. The highly ^{17}O-enriched grain T54 could have formed in an AGB star undergoing hot bottom burning or in a massive star in the Of-WN phase.

O-rich circumstellar dust seems to be underrepresented in meteorites, relative to C-rich. Explanations include the possibility that most O-rich stardust grains are silicates and have been destroyed either in the laboratory or in nature and the possibility that presolar Al_2O_3 has a finer grain size distribution than SiC and graphite.

Subject headings: dust, extinction — meteors, meteoroids — nuclear reactions, nucleosynthesis, abundances — solar system: formation — stars: AGB and post-AGB

1. INTRODUCTION

With the exception of H, He, and some Li, all elements in the solar system were synthesized during various nuclear burning stages in stars. Although the nucleosynthetic processes occurring in different stars generally result in a wide range of isotopic compositions (Clayton 1983), by far most of the material from the many stellar sources that contributed to the protosolar cloud was thoroughly processed and mixed, which resulted in the essentially isotopically homogeneous solar system we know today. However, a small fraction of the original material, in the form of presolar dust grains, survived solar system formation and was trapped in primitive meteorites. From their highly unusual isotopic compositions, compared to that of the solar system as a whole, these presolar grains are inferred to have formed in circumstellar atmospheres or, in some cases, in nova or supernova explosions. As such, they are commonly referred to as "circumstellar" or "stellar" grains, and these terms are used interchangeably with "presolar" in this paper. Because their compositions reflect the isotopic and chemical signatures of their sources, presolar grains provide information about stellar evolution and nucleosynthesis, mixing processes in stars, the physical and chemical conditions of stellar atmospheres, and the chemical evolution of the Galaxy (see reviews by Anders & Zinner 1993 and Ott 1993).

The first types of stellar grains identified in meteorites, and the most extensively studied, include diamond (Lewis et al. 1987; Huss & Lewis 1994a, 1994b), SiC (Bernatowicz et al. 1987; Hoppe et al. 1994a), and graphite (Amari et al. 1990; Amari, Lewis, & Anders 1995b). These carbon-rich phases all carry isotopically anomalous noble gases (Lewis et al. 1987; Lewis, Amari, & Anders 1994; Amari et al. 1995b; Nichols et al. 1991, 1994). They were originally dis-

[1] Present address: Department of Terrestrial Magnetism, Carnegie Institution of Washington, 5241 Broad Branch Road NW, Washington, DC 20015.

covered by using the noble gases as tracers to develop chemical and physical strategies for the concentration of presolar phases in meteoritic residues (Tang & Anders 1988; Amari, Lewis, & Anders 1994). Additional types of presolar grains have since been found, including refractory carbides of Ti, Mo, Zr, and Fe, identified in the transmission electron microscope as subgrains in isotopically anomalous graphite and SiC grains (Bernatowicz et al. 1991; Bernatowicz, Amari, & Lewis 1992; Bernatowicz et al. 1996), presolar Si_3N_4, identified by ion microprobe isotopic measurements (Hoppe et al. 1994b; Nittler et al. 1995b), and the subject of this paper: presolar corundum (Al_2O_3), also identified in the ion probe (Huss et al. 1992; Hutcheon et al. 1994; Nittler et al. 1994; Huss et al. 1994a). An important distinction should be noted between the diamonds and refractory carbide subgrains, which are too small to analyze individually ($\sim$2 nm and 5–200 nm, respectively), and the other presolar phases, which can be large enough ($\gtrsim 1$ μm) to allow isotopic analysis of several elements on individual grains.

The Sun is rich in oxygen, and meteorites are primarily made up of isotopically uniform O-rich phases that formed in the solar nebula. The physical and chemical treatments used to isolate presolar grains in meteorites result in residues rich in refractory, acid-resistant phases (see, e.g., Amari et al. 1994). Whereas most of the carbonaceous dust in these residues is isotopically highly anomalous and apparently of stellar origin, the great majority of oxide grains in the residues are isotopically normal and hence of probable solar system origin. The consequent difficulty in locating rare presolar oxide grains, such as Al_2O_3, has precluded their study at anywhere near the level accorded to presolar SiC or graphite grains. Nevertheless, since oxide grains form under different chemical conditions than C-rich grains, and since a significant fraction of interstellar dust is believed to be O-rich (Whittet 1992), such grains provide unique insights into important astrophysical processes. A total of 42 presolar oxide grains, 41 corundums, and one spinel ($MgAl_2O_4$) have been previously reported in residues of the Murchison (CM), Bishunpur (L3), Orgueil (CI), and Tieschitz (H3.6) meteorites (Huss et al. 1992; Nittler et al. 1993; Huss et al. 1994a; Nittler et al. 1994, 1995a; Huss, Fahey, & Wasserburg 1995a). Most were found using an ion-imaging mapping technique, developed for the Washington University ion microprobe, that allows the automatic identification of grains with highly anomalous O-isotopic compositions (Nittler et al. 1994). Besides being anomalous in O, many of them also have large excesses of ^{26}Mg attributable to the decay of the short-lived radionuclide ^{26}Al ($t_{1/2} = 7.3 \times 10^5$ yr), two grains have ^{25}Mg excesses, and one grain has unusual Ti isotopic ratios (Huss, Fahey, & Wasserburg 1994b). Most of these data are broadly consistent with an origin in O-rich red giant stars, and several recent theoretical studies have attempted to explain the properties of these unusual dust grains in terms of such sources (Boothroyd, Sackmann, & Wasserburg 1994, 1995; Wasserburg, Boothroyd, & Sackmann 1995).

We have performed additional searches for presolar oxide grains in order to address a number of questions:

1. How many distinct groups of presolar oxide grains exist?
2. What are the stellar sources of presolar oxide grains, and what constraints on models of such stars can be obtained from the grains' isotopic compositions?
3. How many stars contributed presolar Al_2O_3 to the solar system?
4. What can we infer about the chemical (isotopic) evolution of the Galaxy from the isotopic compositions of stellar oxide grains?

In this paper, we report the $^{16}O/^{17}O$, $^{16}O/^{18}O$, and inferred $^{26}Al/^{27}Al$ ratios of 45 new presolar Al_2O_3 grains and one new presolar $MgAl_2O_4$ grain extracted from a separate of the Tieschitz ordinary chondrite. A preliminary report of these data has been previously presented in an abstract (Nittler 1996). We discuss the total data set of 88 presolar oxide grains identified to date in the context of the questions listed above. A new technique using these data to constrain the age of our galaxy is described in another paper (Nittler & Cowsik 1997).

2. SAMPLES AND EXPERIMENTAL TECHNIQUES

2.1. *Sample Preparation*

A sample of the Tieschitz meteorite was disaggregated by a freeze-thaw technique and size-separated into less than 100 μm and greater than 100 μm fractions. A mass of 4.5 grams of the less than 100 μm sample was processed using a modification of the procedures developed at the University of Chicago (see, e.g., Amari et al. 1994). The sample was first treated with a toluene-methanol mixture to extract soluble organic material and then reacted several times with HF/HCl (in a ratio of 100:1) in a microwave-heated pressure bomb to dissolve silicates. The resulting residue was treated with chromic acid to remove reactive organic kerogens. After colloidal separation of the presolar microdiamonds in 0.1M NH_3 solution, the remaining material was separated by density and grain size into subsamples enriched in various phases. For this work, the separate with density greater than 2.4 g cm^{-3} was further treated with perchloric acid to produce the final residue, T8. Based on energy dispersive X-ray (EDX) analysis of 109 grains in a JEOL 840 scanning electron microscope (SEM), T8 contains approximately 38% Al_2O_3, 22% $MgAl_2O_4$, 9% Cr-rich oxides, and 23% SiC; the remainder is made up of other phases. For ion probe analysis, T8 grains were deposited in isopropanol suspension on cleaned Au foil. Burma spinel ($MgAl_2O_4$) grains (USNM 135273) were also mounted on the foils, using a micromanipulator, for use as terrestrial isotopic standards.

2.2. *Analysis Techniques*

Grains were analyzed in three stages. First, low mass resolution ion imaging of $^{16}O/^{18}O$ ratios with the Washington University ion microprobe (a modified Cameca IMS-3F) was used to "map" the isotopic compositions of large numbers of oxide grains in order to locate isotopically anomalous presolar grain candidates. Second, candidate grains were located in the SEM, where their chemical compositions were determined by EDX analysis and detailed photomicrographs were taken. Third, candidate grains were relocated in the ion probe and analyzed at high mass resolution for their O- and Mg-Al isotopic compositions. For some analyses, a new ion-imaging/high mass resolution mapping technique was used and will be described below (§ 2.2.3).

2.2.1. *Ion Imaging*

We have previously briefly described the technique of ion imaging (Nittler et al. 1994). The ion optics of the Cameca

IMS-3F ion microprobe are designed such that direct images of mass-selected ions from the sample surface may be obtained at high magnification and high spatial resolution. Negative secondary ions sputtered from the sample surface by Cs^+ ions are separated by mass at low mass resolution in a double-focusing magnetic mass spectrometer and focused onto a dual microchannel plate/fluorescent screen (MCP/FS) detector in such a way that they form an enlarged image of the sample surface. The resulting optical image on the fluorescent screen is digitized to 16 bit precision by a Photometrics 200 series CCD camera. The 512×512 CCD array is binned into a 256×256 pixel image to increase the dynamic range and signal-to-noise ratio. Image processing algorithms are used to assign regions of pixels to individual grains in the ion images. Isotopic ratios for these grains are then determined by ratioing the integrated pixel intensities of these regions in different isotopic images,

The set of isotopes imaged for this study is shown in Table 1. We obtained images in ^{16}O and ^{18}O to search for presolar oxide grains; images in other isotopes (e.g., ^{12}C) were also acquired to aid in relocating grains in the SEM and ion probe. To compensate for changing count rates due to sputtering during long exposures for ^{18}O images, ^{16}O images were acquired both before and after ^{18}O images, and averaged for the determination of isotopic ratios. After each set of images was acquired, the ion probe sample stage was automatically moved to a new location for the next imaging run. Because each imaging run required about 5 minutes and each image contained (typically) 50–100 grains, we were able to determine $^{16}O/^{18}O$ ratios of large numbers of grains much more rapidly, albeit at lower precision, than is possible with standard single grain isotopic measurement techniques.

Sample, 256×256 pixel isotopic ion images of Tieschitz T8 grains, with dark frames subtracted, are shown in Figures 1*a*–1*c* (Plate 12). The ^{16}O and ^{18}O (Figs. 1*a* and 1*b*) image intensities have been scaled for display such that grains with a solar $^{16}O/^{18}O$ ratio (≈ 500) appear similar in both images. The grain marked with an arrow is clearly depleted in ^{18}O and was subsequently confirmed to be a presolar grain. Figure 1*c* shows a ^{28}Si image of the same area of the sample mount; since the Si signal is primarily from SiC and not oxide grains, the Si and O images differ. An SEM micrograph of the same area as in the ion images is shown in Figure 1*e*, and a high-magnification micrograph of the presolar Al_2O_3 grain in this area is shown in Figure 1*f*.

TABLE 1

TYPICAL SET OF ISOTOPES AND EXPOSURE TIMES USED IN ION-IMAGING SEARCHES FOR CIRCUMSTELLAR OXIDE GRAINS

Isotope	Exposure Time (s)
^{12}C	1.0
^{16}O	0.1
^{18}O	50.0
^{16}O	0.1
$^{12}C^{14}N$.....	1.0
^{28}Si	1.0
^{30}Si	30.0
^{28}Si	1.0

NOTE.—Carbon and CN are imaged to aid in locating grains on the sample mount. Images of silicon isotopes are acquired to search for other types of circumstellar grains, especially SiC grains X and Si_3N_4 (Nittler et al. 1995b). Exposure times for each isotope are chosen for optimal image brightness.

The contours shown in Figure 1*d* indicate grain boundaries defined for the O-isotope images by a "particle-definition" program. For each grain in an image, this algorithm expands radially around the brightest pixel (local maximum in pixel intensity), assigning to the grain all neighboring pixels with intensities above a threshold (typically 35% of the maximum). To distinguish close grains, only pixels for which the image intensity decreases monotonically in the radial direction away from the grain center are included in a given grain. Isotopic ratios of defined grains were quantitatively determined from image intensities by the formula

$$\frac{^{16}O}{^{18}O} = \left(\frac{I_{16}}{T_{16}} \cdot \frac{T_{18}}{I_{18}}\right)^n, \quad (1)$$

where I_i is the average intensity of pixels within the defined contour in the image of mass i, T_i is the exposure time of image i, and n (≈ 0.96) is a correction exponent needed to compensate for nonlinearity of the MCP/FS detector. Such nonlinearity is probably the result of electrons from a single channel in the first MCP spreading into multiple channels in the second plate, which gives rise to an apparent "gain" for high count rates (Hunter, Linton, & Griffis 1991). The nonlinearity exponent n was determined by comparing secondary ion signals, measured with an electron multiplier, with image intensities for a wide range of count rates. Because ion images are acquired at low mass-resolving power, hydride ions from residual water on the sample mount contribute to the ^{18}O images and lead to measured $^{16}O/^{18}O$ ratios lower than the true ratios. This effect is important for small grains for which the background is relatively high, and was corrected for by fitting curves to plots of $^{16}O/^{18}O$ ratios versus image intensities (small grains have lower intensities). After data correction, Gaussians were fitted to histograms of measured $^{16}O/^{18}O$ ratios, and grains that deviated by more than 3 σ ($\sigma \approx 3\%$–5%; see § 3.1) from the mean were identified as presolar grain candidates.

2.2.2. *Isotopic Measurements*

Subsequent to SEM characterization, presolar grain candidates were analyzed as individual grains in the ion microprobe, following standard (i.e., not imaging) high mass resolution isotopic ratio measurement techniques (see, e.g., McKeegan, Walker, & Zinner 1985). The ion probe was operated in an automatic peak-jumping mode, using an electron multiplier to detect secondary ions. Burma spinel ($MgAl_2O_4$) standards were used to determine instrumental mass fractionation corrections for measured isotopic ratios and to center mass peaks. All three stable O isotopes were measured as negative secondary ions produced by a Cs^+ primary ion beam, and Al and Mg were measured as positive secondary ions produced by O^- bombardment. Because many of the candidate grains were too small to

survive both the ion-imaging and the high mass resolution O-isotopic measurement, Al and Mg were measured only in a subset of the presolar grains.

The technique for measuring O-isotopic ratios in oxide grains has been described previously by McKeegan (1987). Analyses were made at a mass-resolving power of ~ 5000, which is sufficient to resolve $^{17}O^-$ ions from $^{16}OH^-$ ions, and the latter were collected along with ions of the three oxygen isotopes. Although the magnetic field settings for all of the measured peak centers were determined on the Burma spinel standards, only the $^{16}O^-$ peak was centered on the smaller meteoritic grains because count rates of the rare isotopes were very low. Shifts in the ^{16}O peak position were used to determine peak shift corrections for the other isotopes. The $^{16}OH^-$ signal was typically 10–100 times as high as the $^{17}O^-$ signal and was found to come primarily from residual water on the sample mount and not from the grains. To check that the tail of the $^{16}OH^-$ peak did not significantly contribute to the ^{17}O peak, measurements of presolar grain candidates were interspersed with measurements of noncandidate grains, under identical conditions. These measurements indicate that ^{16}OH contributions to the ^{17}O signal were well below the analytical uncertainty due to counting statistics. A masking aperture was used during all measurements to block contributions from nearby grains, but in a few cases, such contributions were unavoidable, and the true isotopic compositions of some of the grains thus may be even more extreme than reported.

Magnesium isotopes and Al were measured following the techniques described by McKeegan et al. (1985), Fahey et al. (1987), and Virag et al. (1991). A mass-resolving power of 3000, sufficient to resolve all important interferences, was used. As in the case of the O-isotopic measurements, peak centering for the three Mg isotopes and Al was carried out on the Burma spinel standards, and only the $^{27}Al^+$ peak was centered during measurements of the meteoritic Al_2O_3 grains, because Mg concentrations were low ($Mg/Al = 10^{-4}$ to 10^{-2}). Measured Mg isotopic ratios were corrected for instrumental mass fractionation, based on Burma spinel analyses. The measured $^{26}Mg/^{24}Mg$ ratios were not corrected for "intrinsic" mass fractionation, however, both because errors on $^{25}Mg/^{24}Mg$ measurements were large and because deviations of the $^{25}Mg/^{24}Mg$ ratio from normal, if present, are not necessarily due to mass dependent isotopic fractionation but could be the result of nucleosynthetic effects. Since $^{25}Mg/^{24}Mg$ ratios were normal (within the large errors) in all of the grains, we ascribe observed ^{26}Mg excesses to in situ decay of ^{26}Al after grain formation. Initial $^{26}Al/^{27}Al$ ratios were inferred for the grains using the formula

$$\frac{^{26}Al}{^{27}Al} = \left[\frac{(^{26}Mg/^{24}Mg)_{grain} - (^{26}Mg/^{24}Mg)_{std}}{^{27}Al^+/^{24}Mg^+ \times \Lambda}\right]. \quad (2)$$

The standard $^{26}Mg/^{24}Mg$ ratio was taken to be 0.13932 following Catanzaro et al. (1966). The sensitivity factor Λ relating the measured $^{27}Al/^{24}Mg$ ion ratio to the true ratio was taken to be 1.44, based on Burma spinel analyses. In several cases, we were unable to mask completely Mg and/or Al contributions from nearby grains during a measurement. The addition of isotopically normal Mg does not affect the inferred $^{26}Al/^{27}Al$ ratio, but extra Al will decrease the inferred ratio from its true value. In such cases, secondary ion images of Mg and Al were acquired and the contribution of "extra" Al estimated and corrected from these images.

2.2.3. *High Mass Resolution Mapping*

Imaging of ^{17}O is not practical with our ion-imaging system, owing both to the low natural abundance of this isotope and to the high mass resolving power needed to separate ^{16}OH ions. Prior work has shown, however, that some presolar oxide grains have extremely anomalous $^{16}O/^{17}O$ ratios but normal $^{16}O/^{18}O$ ratios (Huss et al. 1994a, 1995b). These grains would be missed by the ion-imaging mapping technique described above, which identifies grains with anomalous $^{16}O/^{18}O$ ratios. To determine what fraction of presolar oxide grains are missed by mapping in $^{16}O/^{18}O$, we developed a "semi-automated" method for high mass resolution $^{16}O/^{17}O$ ratio measurements. Ion imaging was used to map a Tieschitz T8 grain mount (labeled T8E1) in $^{16}O^-$ and $^{27}Al^{16}O^-$ ions, and image processing was used to determine the coordinates of individual Al-rich oxide grains on the mount. Because we did not image in ^{18}O, total exposure times were kept short with consequently little sputtering of the grains prior to high mass resolution analysis. With the coordinates of grains automatically determined in this way, we analyzed the grains one by one, performing a short measurement of $^{16}O/^{17}O$ and $^{16}O/^{18}O$ ratios on each one. Total counting times for ^{16}O, ^{17}O, and ^{18}O were 3, 18, and 15 seconds, respectively. The total time for each grain measurement, including locating the grain, centering the primary ion beam and counting secondary ions, was less than 3 minutes, and the 2 σ analytical uncertainty (due to counting statistics) was typically 20% for $^{17}O/^{16}O$ and 10% for $^{18}O/^{16}O$. Grains that appeared anomalous during a short analysis were immediately measured at higher precision.

3. RESULTS

3.1. *Ion Imaging*

For this study, we acquired images of 410 separate 100×100 μm areas of a Tieschitz T8 grain mount (labeled T8D1) in the isotopes shown in Table 1. A total of $\approx 35{,}000$ grains were defined in the images. A number of criteria were used to restrict this data set. Grains were eliminated if their ion signals saturated the detector, if count rates changed significantly faster than average owing to sputter loss (monitored by examining intensities in the first and second ^{16}O images), if they appeared to be artifacts of the particle-definition algorithm, or if they had too high a background contribution to yield a reliable isotopic measurement. The resulting data of the remaining 17,000 grains, corrected for detector nonlinearity and background as described in § 2.2.1, are presented in Figure 2. In this figure, the measured $^{16}O/^{18}O$ ratio, divided by the solar ratio of 499, is plotted against the average ^{16}O image intensity (I_{16} in eq. [1]), for each grain in the data set. Most of the grains have measured ratios close to the solar ratio, but as can be clearly seen, the variation about the solar ratio is larger for small grains (low intensity) than for large ones (high intensity). The width of the distribution of measured ratios is determined by both the analytical uncertainties and the intrinsic $^{16}O/^{18}O$ distribution of Tieschitz refractory oxide grains, but the increased width at low intensity is probably due to larger counting-statistical errors for small grains than for large grains. The solid curves indicate 3 σ limits obtained by

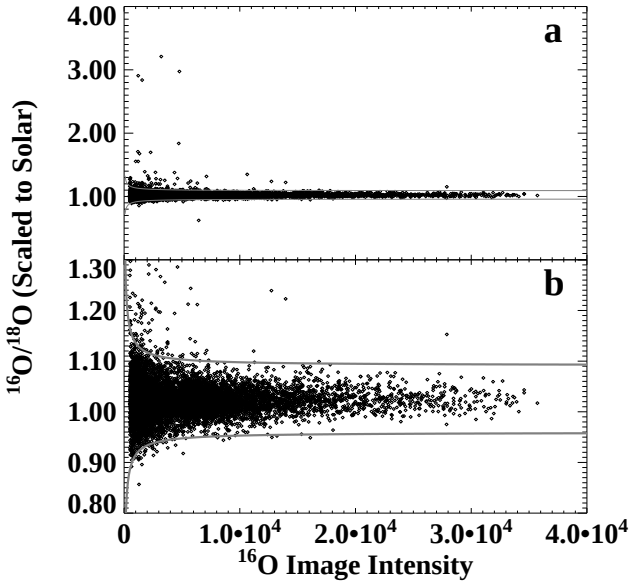

FIG. 2.—$^{16}O/^{18}O$ ratios measured in 17,000 Tieschitz oxide grains by ion imaging, plotted against the average intensity in ^{16}O ion images. The $^{16}O/^{18}O$ ratios are divided by the solar value of 499. Shown in (*a*) is the entire data set; in (*b*), an expanded view of the $^{16}O/^{18}O = 0.8$–1.3 region. Gray curves indicate 3 σ limits, where σ is the intensity-dependent standard deviation of the main ratio distribution. Grains outside these curves were identified as presolar grain candidates and were chosen for high-mass-resolution analysis.

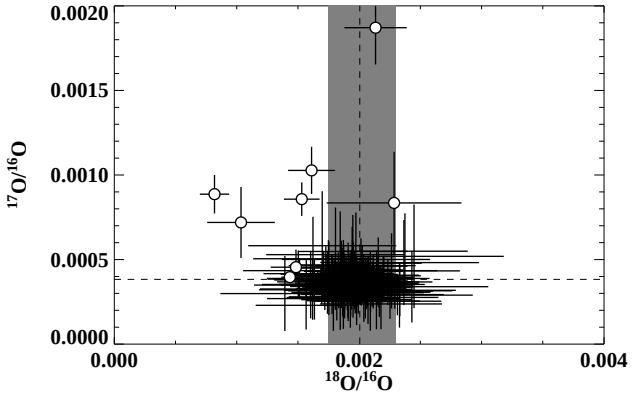

FIG. 3.—Results of low-precision O-isotopic measurements of 403 acid-resistant oxide grains from the Tieschitz meteorite. Error bars are 2 σ; dashed lines indicate solar isotopic ratios in this and subsequent figures. The shaded region denotes the approximate range of $^{18}O/^{16}O$ of the bulk of ion-imaging measurements (main distribution in Fig. 2); presolar grains within this region would not be selected as presolar grain candidates from the ion-imaging data. The eight grains marked by open circles are highly anomalous and thus identified as circumstellar grains. Since two to four of these have $^{18}O/^{16}O$ ratios in or at the edge of the shaded region, we infer that one-fourth to one-half of presolar oxide grains in Tieschitz are missed by ion-imaging searches for grains anomalous in $^{18}O/^{16}O$.

a fit to the standard deviation of the main distribution as a function of image intensity. These 3 σ limits range from $\sim$13% for the smallest grains to $\sim$9% for the largest. Grains that lie outside the 3 σ limits were chosen as presolar grain candidates.

Of the 60 candidate grains chosen for high mass resolution analysis, 38 were confirmed to have isotopic compositions that differed in at least one isotopic ratio by greater than 2 σ from the known range of O-isotopic compositions in meteorites (excluding presolar grains). We consider these grains to have a circumstellar origin (see § 3.4). The remainder of the candidates were either sputtered away by the primary ion beam before they could be remeasured, were too close to other grains to be adequately analyzed as distinct grains, or turned out to be isotopically normal on remeasurement. We note that the candidate grains that proved to be normal were all close to the 3 σ curves shown in Figure 2, and their "anomalous" $^{16}O/^{18}O$ ratios obtained by ion imaging are probably the result of statistical fluctuations.

3.2. *High Mass Resolution Mapping*

The O-isotopic ratios of 403 Tieschitz T8E1 Al_2O_3 and $MgAl_2O_4$ grains, obtained with the "semi-automated" mapping technique described in § 2.2.3, are shown in Figure 3. A total of 500 grains were identified by imaging of O and AlO secondary ions and were subjected to a short high mass resolution measurement. However, 97 of these grains had secondary ion signals that changed by more than 60% during the short measurement, and their data are not shown in the figure. Eight of the remaining grains (open symbols in Fig. 3) have O-isotopic ratios indicative of a circumstellar origin, confirmed by subsequent full measurements. The shaded area in Figure 3 shows the approximate range of $^{18}O/^{16}O$ ratios measured by ion imaging in the bulk of oxide grains from Tieschitz; presolar grains must lie outside this region to be identified by ion imaging. Two of the circumstellar grains in Figure 3 fall in the shaded region, and two fall well outside of it ($^{18}O/^{16}O \lesssim 0.001$). Of the other four presolar grains, two have large ^{17}O enrichments and $^{18}O/^{16}O$ ratios close to the ion-imaging limit, and two have approximately normal $^{17}O/^{16}O$ ratios and intermediate ^{18}O depletions ($^{18}O/^{16}O \sim 0.0015$). Depending on whether or not the grains at the edge of the shaded region would be identified as anomalous by ion imaging, these data indicate that from one-fourth to one-half of presolar oxide grains in Tieschitz have ^{17}O enrichments greater than $\sim$30% but $^{18}O/^{16}O$ ratios close enough to solar to be missed by ion-imaging mapping of $^{16}O/^{18}O$ ratios. We note, however, that the grains that are missed belong to the best understood group of presolar oxides (see § 4).

3.3. *Sizes and Morphologies*

SEM-EDX analysis of the T8D1 circumstellar grains revealed only Al and O X-ray peaks in all but one grain, T44, which also has a Mg peak. The grains are thus inferred to be corundum (Al_2O_3), with the exception of T44, which is spinel ($MgAl_2O_4$). Unlike the previously reported presolar spinel grain, T3, which had a lower than typical Mg/Al ratio (Nittler et al. 1994), the EDS spectrum of T44 is similar to that obtained on a terrestrial spinel standard.

The size distribution of the T8D1 presolar oxide grains, estimated from SEM micrographs, is shown in Figure 4. For round grains, the given size is the diameter. For non-round grains, the size was taken as $2 \times (A/\pi)^{1/2}$, where A is the estimated cross-sectional area of the grain. The darker region indicates 10 candidate grains that had highly anomalous $^{16}O/^{18}O$ ratios according to their ion images but that were either too small or could not be sufficiently distinguished from neighboring grains to be analyzed at high mass resolution. The size distribution in Figure 4 probably differs from the true distribution within the meteorite for several reasons. First, the grains have been sputtered somewhat during ion imaging. The observed size of a grain thus

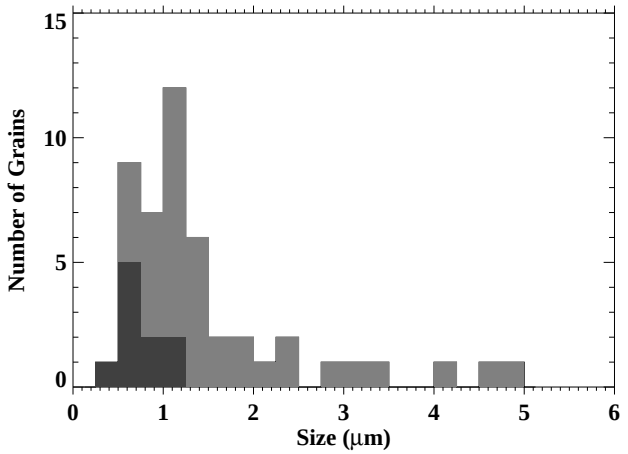

FIG. 4.—Size distribution of circumstellar oxide grains from Tieschitz sample mount T8D1. The darker region indicates 10 grains for which ion imaging indicated isotopically highly anomalous $^{16}O/^{18}O$ ratios but which could not be analyzed at high mass resolution. Most presolar oxide grains in our Tieschitz residues are very small ($\lesssim 1.5$ μm), which limits the amount of material available for isotopic ratio measurements.

depends on the extent of this sputtering, which is likely to vary from grain to grain owing to geometry effects. Second, the ion-imaging technique used to find presolar grains is more sensitive to larger grains, which have smaller analytical uncertainty and lower relative background contributions. Finally, the chemical treatments used to prepare the Tieschitz residue are likely preferentially to destroy or lose small oxide grains relative to large ones. Even if the measured distribution does reflect that in the meteorite, however, it is unlikely to be the same as in the stellar sources, since small grains were probably preferentially destroyed during passage from their sources to the solar system. In any case, it is clear from Figure 4 that most of the circumstellar oxide grains in Tieschitz T8 are $\lesssim 1.5$ μm in diameter. Because of their small sizes and because Al_2O_3 takes up trace elements less readily than SiC or graphite, isotopic studies of elements other than O and Mg in single circumstellar oxide grains are difficult at present.

Because the presolar oxide grains of this study have been sputtered by an ion beam prior to SEM examination, it is difficult to ascertain what their original morphologies were. Moreover, the small sizes of most of the grains (Fig. 4) make it difficult to distinguish surface textures. Nevertheless, the presolar oxide grains appear, in general, quite similar to most circumstellar SiC grains found in meteorites (Hoppe et al. 1994a) (see Fig. 1*f*). Many show well-defined crystal surfaces. The grains frequently appear to have tiny grains on their surfaces, but whether these are real subgrains or unrelated grains from the Tieschitz separate is unknown.

3.4. *Isotopic Compositions*

The $^{17}O/^{16}O$, $^{18}O/^{16}O$, and inferred initial $^{26}Al/^{27}Al$ ratios for the new circumstellar oxide grains from Tieschitz, T38–T83, are given in Table 2. Ratios for Tieschitz grains T22–T37, which have been previously presented in graphical form in Nittler et al. (1995a), are also included. Not shown in the table, but included in figures and discussion, are Tieschitz grains T1–T21, Murchison grain 83-5, Orgueil grain B, and Bishunpur grains B39, B155, and B1299 (Nittler et al. 1994; Huss et al. 1994a; G. Huss, private communication).

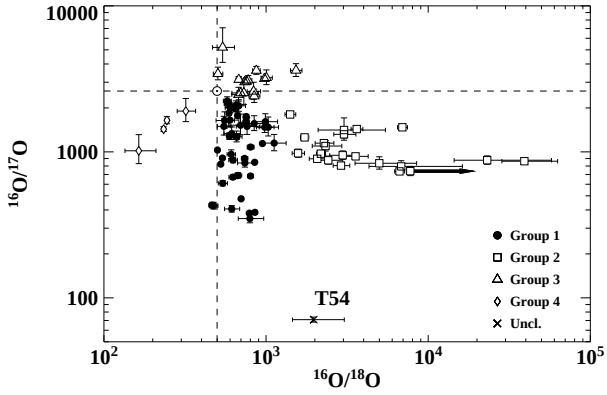

FIG. 5.—$^{16}O/^{17}O$ and $^{16}O/^{18}O$ ratios (1 σ errors) of 88 circumstellar oxide grains extracted from primitive meteorites. The grains have been divided into four groups on the basis of this plot; see text and Table 3 for group definitions. Grain T54 is unlike any others and is not assigned to a group.

3.4.1. *O Isotopes*

The O-isotopic compositions of 87 of the 88 presolar oxide grains that have been found to date are shown in Figure 5, plotted as $^{16}O/^{18}O$ versus $^{16}O/^{17}O$ ratios. The grains have been divided into four groups on the basis of this plot; see Table 3. One grain, T75, was inadvertently not analyzed for $^{16}O/^{17}O$, but its $^{16}O/^{18}O$ (determined by ion imaging) and inferred $^{26}Al/^{27}Al$ ratios are given in Table 2. Logarithmic scales are used in Figure 5 to cover the enormous range of compositions exhibited by the grains; the observed range of O-isotopic compositions in the solar system, excluding presolar grains, falls within the solar symbol. Figure 6 presents most of the data on a linear scale; the inverse ratios of those of Figure 5 are shown for clarity. In previous reports of presolar oxide grains, we divided the data into four distinct groups on the basis of their O-isotopic ratios (Nittler et al. 1994, 1995a). We shall continue to divide the grains into these groups as an aid to the discussion; the isotopic properties of the four groups are summarized in Table 3. We do so with the caution that the assignment of a particular grain to a particular group is somewhat arbitrary in many cases. General O-isotopic trends are quite clear, however, and probably reflect different processes operating in the parent stars of the grains.

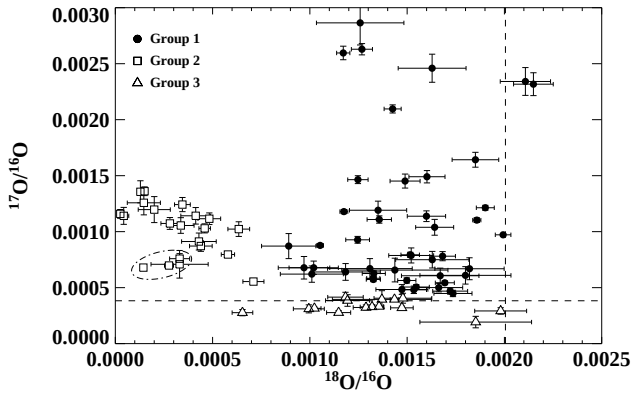

FIG. 6.—$^{17}O/^{16}O$ and $^{18}O/^{16}O$ ratios of presolar oxide grains belonging to Groups 1–3. In contrast to Fig. 5, data are plotted on a linear scale. Dash-dotted ellipse surrounds four Group 2 grains that may be distinct from the main Group 2 trend.

TABLE 2

ISOTOPIC COMPOSITIONS OF CIRCUMSTELLAR OXIDE GRAINS[a]

Grain	Group	$^{17}O/^{16}O$	$^{18}O/^{16}O$	$^{26}Al/^{27}Al$
Solar.....		3.83×10^{-4}	2.004×10^{-3}	...
T22	4	$6.99\ (26) \times 10^{-4}$	$4.28\ (12) \times 10^{-3}$	$< 1.7 \times 10^{-3}$
T23	3	$3.20\ (15) \times 10^{-4}$	$1.47\ (6) \times 10^{-3}$	$1.34\ (66) \times 10^{-4}$
T24	1	$6.26\ (24) \times 10^{-4}$	$1.33\ (6) \times 10^{-3}$	$6.8\ (1.3) \times 10^{-3}$
T25	2	$1.36\ (10) \times 10^{-3}$	$< 1.29 \times 10^{-4}$	$1.65\ (33) \times 10^{-2}$
T26	2	$5.54\ (28) \times 10^{-4}$	$7.10\ (54) \times 10^{-4}$	$1.95\ (46) \times 10^{-3}$
T27	2	$7.96\ (23) \times 10^{-4}$	$5.79\ (34) \times 10^{-4}$	$1.05\ (8) \times 10^{-3}$
T28	1	$9.27\ (30) \times 10^{-4}$	$1.25\ (6) \times 10^{-3}$	$< 1.6 \times 10^{-5}$
T29	1	$5.84\ (13) \times 10^{-4}$	$1.33\ (3) \times 10^{-3}$	n.m.[b]
T30	1	$4.69\ (27) \times 10^{-4}$	$1.72\ (9) \times 10^{-3}$	n.m.
T31	3	$4.05\ (44) \times 10^{-4}$	$1.48\ (15) \times 10^{-3}$	$6.16\ (64) \times 10^{-4}$
T32	1	$6.06\ (68) \times 10^{-4}$	$1.67\ (20) \times 10^{-3}$	n.m.
T33	4	$5.26\ (95) \times 10^{-4}$	$3.13\ (41) \times 10^{-3}$	n.m.
T34	4	$9.8\ (2.2) \times 10^{-4}$	$6.1\ (1.3) \times 10^{-3}$	$1.12\ (15) \times 10^{-3}$
T35	1	$6.40\ (75) \times 10^{-4}$	$1.18\ (18) \times 10^{-3}$	n.m.
T36	1	$1.21\ (2) \times 10^{-3}$	$1.90\ (5) \times 10^{-3}$	$< 1.3 \times 10^{-4}$
T37	2	$8.71\ (47) \times 10^{-4}$	$4.40\ (58) \times 10^{-4}$	$< 2.4 \times 10^{-4}$
T38	1	$4.84\ (44) \times 10^{-4}$	$1.47\ (13) \times 10^{-3}$	n.m.
T39	2	$1.12\ (5) \times 10^{-3}$	$4.83\ (58) \times 10^{-4}$	$3.47\ (11) \times 10^{-3}$
T40	1	$2.10\ (4) \times 10^{-3}$	$1.43\ (4) \times 10^{-3}$	$< 6.2 \times 10^{-4}$
T41	2	$1.07\ (5) \times 10^{-3}$	$2.81\ (46) \times 10^{-4}$	$1.38\ (3) \times 10^{-2}$
T42	2	$6.98\ (22) \times 10^{-4}$	$2.76\ (23) \times 10^{-4}$	$8.83\ (10) \times 10^{-3}$
T43	1	$4.48\ (28) \times 10^{-4}$	$1.74\ (10) \times 10^{-3}$	n.m.
T44	1	$6.70\ (89) \times 10^{-4}$	$1.31\ (22) \times 10^{-3}$	n.m.
T45	3	$2.77\ (17) \times 10^{-4}$	$1.15\ (6) \times 10^{-3}$	$< 5.0 \times 10^{-4}$
T46	1	$2.46\ (13) \times 10^{-3}$	$1.63\ (17) \times 10^{-3}$	$< 3.4 \times 10^{-4}$
T47	2	$1.05\ (7) \times 10^{-3}$	$3.37\ (68) \times 10^{-4}$	$4.13\ (20) \times 10^{-3}$
T48	2	$7.1\ (1.2) \times 10^{-4}$	$3.3\ (1.5) \times 10^{-4}$	n.m.
T49	1	$1.64\ (7) \times 10^{-3}$	$1.85\ (12) \times 10^{-3}$	$6.83\ (83) \times 10^{-4}$
T50	2	$7.59\ (45) \times 10^{-4}$	$3.31\ (51) \times 10^{-4}$	$2.11\ (10) \times 10^{-3}$
T51	3	$3.95\ (78) \times 10^{-4}$	$1.37\ (25) \times 10^{-3}$	$< 2.0 \times 10^{-4}$
T52	1	$2.86\ (20) \times 10^{-3}$	$1.26\ (22) \times 10^{-3}$	$6.4\ (1.3) \times 10^{-4}$
T53	2	$1.14\ (7) \times 10^{-3}$	$4.13\ (77) \times 10^{-4}$	n.m.
T54	...	$1.41\ (5) \times 10^{-2}$	$5.0\ (2.0) \times 10^{-4}$	n.m.
T55	2	$1.20\ (12) \times 10^{-3}$	$2.00\ (82) \times 10^{-4}$	n.m.
T56	1	$1.46\ (4) \times 10^{-3}$	$1.25\ (5) \times 10^{-3}$	$1.20\ (5) \times 10^{-3}$
T57	1	$6.10\ (78) \times 10^{-4}$	$1.80\ (23) \times 10^{-3}$	n.m.
T58	2	$1.16\ (4) \times 10^{-3}$	$2.55\ (96) \times 10^{-5}$	$9.46\ (19) \times 10^{-3}$
T59	1	$6.78\ (59) \times 10^{-4}$	$1.02\ (13) \times 10^{-3}$	n.m.
T60	1	$6.21\ (73) \times 10^{-4}$	$1.01\ (16) \times 10^{-3}$	n.m.
T61	4	$6.08\ (34) \times 10^{-4}$	$4.09\ (11) \times 10^{-3}$	$3.10\ (6) \times 10^{-3}$
T62	3	$3.85\ (52) \times 10^{-4}$	$1.19\ (11) \times 10^{-3}$	n.m.
T63	1	$8.7\ (1.1) \times 10^{-4}$	$8.9\ (1.4) \times 10^{-4}$	n.m.
T64	3	$3.10\ (36) \times 10^{-4}$	$9.95\ (80) \times 10^{-4}$	$2.86\ (53) \times 10^{-4}$
T65	2	$1.24\ (6) \times 10^{-3}$	$3.45\ (40) \times 10^{-4}$	n.m.
T66	3	$4.15\ (44) \times 10^{-4}$	$1.18\ (9) \times 10^{-3}$	$< 6.6 \times 10^{-4}$
T67	3	$2.77\ (28) \times 10^{-4}$	$6.53\ (53) \times 10^{-4}$	$4.03\ (76) \times 10^{-4}$
T68	1	$1.45\ (6) \times 10^{-3}$	$1.49\ (8) \times 10^{-3}$	$< 1.6 \times 10^{-4}$
T69	1	$1.18\ (2) \times 10^{-3}$	$1.17\ (2) \times 10^{-3}$	$2.79\ (4) \times 10^{-3}$
T70	1	$7.87\ (67) \times 10^{-4}$	$1.52\ (12) \times 10^{-3}$	n.m.
T71	1	$5.73\ (20) \times 10^{-4}$	$1.33\ (4) \times 10^{-3}$	$6.12\ (10) \times 10^{-3}$
T72	1	$5.64\ (23) \times 10^{-4}$	$1.50\ (5) \times 10^{-3}$	$1.63\ (4) \times 10^{-3}$
T73	1	$8.77\ (15) \times 10^{-4}$	$1.05\ (2) \times 10^{-3}$	$1.83\ (3) \times 10^{-3}$
T74	3	$3.32\ (8) \times 10^{-4}$	$1.36\ (2) \times 10^{-3}$	$< 4.0 \times 10^{-5}$
T75	...	n.m.	$< 1.43 \times 10^{-4}$	$1.84\ (13) \times 10^{-3}$
T76	1	$6.69\ (98) \times 10^{-4}$	$1.82\ (18) \times 10^{-3}$	n.m.
T77	2	$1.03\ (4) \times 10^{-3}$	$4.59\ (30) \times 10^{-4}$	n.m.
T78	1	$2.34\ (12) \times 10^{-3}$	$2.11\ (13) \times 10^{-3}$	n.m.
T79	1	$7.81\ (41) \times 10^{-4}$	$1.68\ (7) \times 10^{-3}$	n.m.
T80	3	$3.95\ (10) \times 10^{-4}$	$1.43\ (2) \times 10^{-3}$	n.m.
T81	1	$6.8\ (1.0) \times 10^{-4}$	$9.7\ (1.3) \times 10^{-4}$	n.m.
T82	1	$1.04\ (7) \times 10^{-3}$	$1.64\ (10) \times 10^{-3}$	n.m.
T83	1	$4.81\ (33) \times 10^{-4}$	$1.53\ (7) \times 10^{-3}$	n.m.

[a] All errors are 1 σ.

[b] "n.m." means "not measured."

Most of the presolar oxide grains lie in the lower right quadrant of Figure 5 corresponding to lower than solar $^{16}O/^{17}O$ and higher than solar $^{16}O/^{18}O$ ratios (enriched ^{17}O and depleted ^{18}O). A histogram of the $^{18}O/^{16}O$ ratios for the grains in this quadrant is shown in the top panel of Figure 7. The distribution is double-peaked, and we have divided these grains into two separate groups on the basis of this plot. Group 1 grains have solar $^{16}O/^{18}O$ or moderate ^{18}O depletions ($^{16}O/^{18}O < 1250$; $^{18}O/^{16}O > 0.0008$), whereas Group 2 grains have much more extreme ^{18}O

TABLE 3

GROUPS OF CIRCUMSTELLAR OXIDE GRAINS

GROUP	NUMBER	$^{16}O/^{17}O$ RANGE	$^{16}O/^{18}O$ RANGE	FRACTION WITH ^{26}Al	$^{26}Al/^{27}Al$	
					Range	Mean
1	46	349–2232	465–1122	16/23	0.00012–0.0078	0.0023
2	21	735–1804	1409–∞	12/13	0.001–0.016	0.0060
3	15	2409–5195	505–1530	4/11	0.00013–0.00062	0.0004
4	4	1017–1902	164–320	2/3	0.001–0.0031	0.0021

depletions ($^{16}O/^{18}O > 1250$; $^{18}O/^{16}O < 0.0008$). Besides having lower $^{18}O/^{16}O$ ratios, Group 2 grains also differ from Group 1 in their much narrower range of $^{17}O/^{16}O$ ratios (Table 2 and Fig. 6). Note that most circumstellar Al_2O_3 grains with solar $^{16}O/^{18}O$ ratios belong to Group 1. The results presented in § 3.2 indicate that Group 1 grains are underrepresented in this data set compared to their true proportion in the population of circumstellar oxide grains in the Tieschitz meteorite by a factor of ~1.5–3.

The remaining two groups of circumstellar Al_2O_3 grains fall in different quadrants of Figure 5. Grains that have solar or smaller than solar $^{17}O/^{16}O$ ratios are assigned to Group 3. The bottom panel of Figure 7 shows that Group 3 grains tend to have $^{18}O/^{16}O$ ratios that overlap with the lower range of the Group 1 distribution. Exceptions are the two previously reported grains T3 and T8, which have solar $^{18}O/^{16}O$ ratios (Nittler et al. 1994), and grain T67, with $^{18}O/^{16}O = 0.00065$. Using the solar $^{17}O/^{16}O$ ratio as the dividing line between Groups 1 and 3 is somewhat arbitrary as there is no clear break in the O-isotopic distribution at this ratio. However, the distributions of inferred $^{26}Al/^{27}Al$ ratios are clearly different for the two groups (§ 3.4.2), lending some support to dividing the data in this way. The four grains with highly enriched ^{18}O and ^{17}O, relative to solar, are classified as belonging to Group 4.

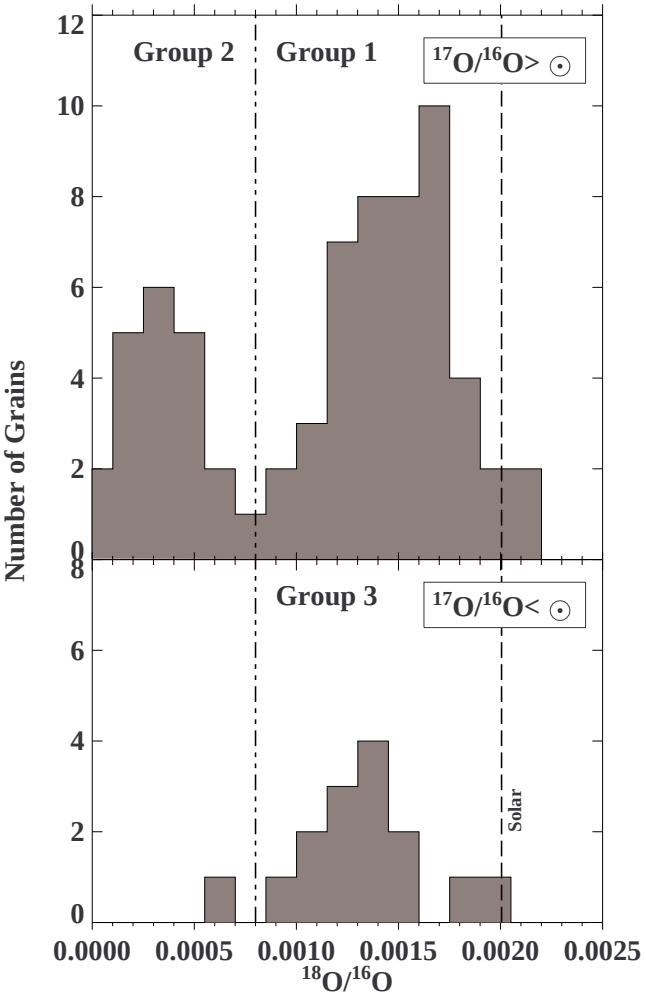

FIG. 7.—Histogram of $^{18}O/^{16}O$ ratios of circumstellar oxide grains belonging to Groups 1–3. The distribution for grains with $^{17}O/^{16}O$ greater than the solar value has a minimum at ~0.0008, and this value is used to distinguish Group 1 and Group 2 grains. $^{18}O/^{16}O$ ratios of Group 3 grains ($^{17}O/^{16}O \leq$ solar) overlap the lower end of Group 1.

One grain, T54, has an $^{17}O/^{16}O$ ratio 37 times the solar value. Its $^{16}O/^{17}O$ ratio of 71 is lower than any that has been previously observed in natural samples. The measured $^{16}O/^{18}O$ ratio for T54 is about 2000, but is consistent at a 2.5 σ level with ∞. The few ^{18}O ions counted during the measurement could have been from neighboring grains or residual oxygen on the sample mount. Unfortunately, the grain was completely destroyed during the measurement, and we cannot unambiguously decide the question. In any case, T54 is not obviously related to Groups 1 through 4, and we will treat it separately.

3.4.2. *Mg-Al Isotopes*

Seventeen of the 24 new presolar oxide grains analyzed for Mg-Al have large ^{26}Mg excesses (with $^{26}Mg/^{24}Mg$ ratios up to 300 times the solar ratio), but normal $^{25}Mg/^{24}Mg$ ratios. These excesses are almost certainly due to the *in situ* decay of ^{26}Al that was present in the grains when they formed. Inferred initial $^{26}Al/^{27}Al$ ratios for these grains are given in Table 2; 2 σ upper limits are given for grains that did not have measurable excesses of ^{26}Mg. Combining the new data with previously reported Al-Mg measurements of presolar oxide grains (Hutcheon et al. 1994; Nittler et al. 1994, 1995a), we find that 35 of 52 grains measured for Al-Mg have evidence for ^{26}Al, with inferred $^{26}Al/^{27}Al$ ratios between 1.2×10^{-4} and 1.6×10^{-2}.

All of the new circumstellar grains analyzed for Mg-Al have $^{25}Mg/^{24}Mg$ ratios that are solar within the analytical uncertainties. However, Huss et al. (1994b) have previously reported a ~25% excess of ^{25}Mg, relative to solar, in the presolar Al_2O_3 grain Orgueil B. In addition, Tieschitz grain T22 has $^{25}Mg/^{24}Mg = 0.1430(46)$ and $^{26}Mg/^{24}Mg = 0.1722(53)$ (Nittler et al. 1995a). These ratios are ~13% and ~24% larger, respectively, than the solar ratios ($^{25}Mg/^{24}Mg = 0.12663$, $^{26}Mg/^{24}Mg = 0.13932$; Catanzaro et al. 1966). Because the isotopic anomalies of both rare Mg isotopes are similar in magnitude in grain T22, we cannot ascribe the ^{26}Mg excess in this grain to the decay of ^{26}Al (nor can we rule it out). Assuming that the ^{26}Mg is in fact due to ^{26}Al decay, grain T22 has an inferred initial $^{26}Al/^{27}Al$ ratio of 1.3×10^{-3}, and this value is given as an upper limit in Table 2. As this grain is one of the rare Group 4

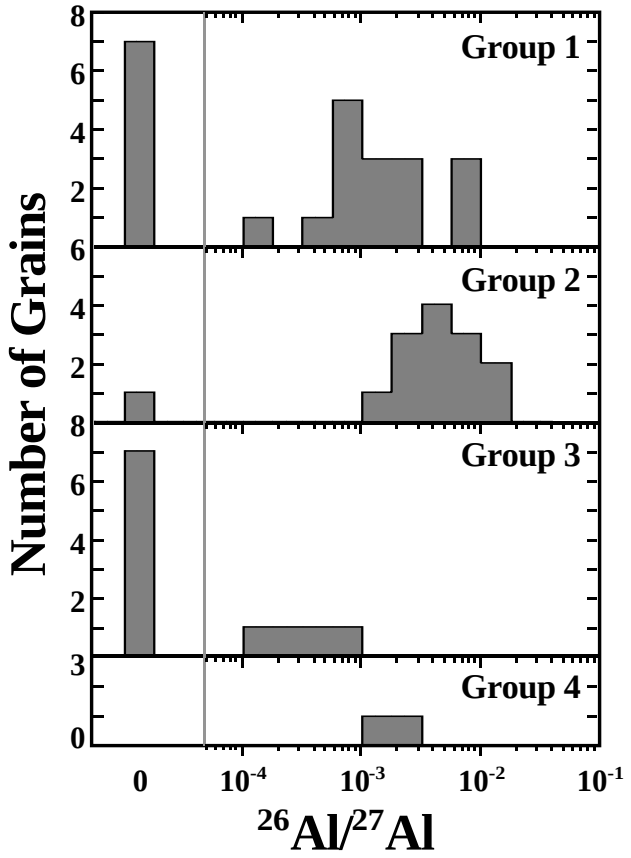

FIG. 8.—Initial $^{26}Al/^{27}Al$ ratios inferred from ^{26}Mg excesses of circumstellar oxide grains, divided into groups according to their O-isotopic ratios. Peaks at $^{26}Al/^{27}Al = 0$ indicate grains without evidence for the original presence of ^{26}Al. The vertical line corresponds to the apparent upper limit of $^{26}Al/^{27}Al = 5 \times 10^{-5}$ observed in early solar system condensates (MacPherson, Davis, & Zinner 1995). The distributions are apparently different for the different groups, in particular the fraction of grains with ^{26}Mg excesses.

grains, we will discuss its unusual Mg isotopic composition in more detail below.

The division of the presolar grains into subgroups based on their O-isotopes (previous section) seems to extend to inferred $^{26}Al/^{27}Al$ ratios. This can be seen in Figure 8, where histograms of the inferred $^{26}Al/^{27}Al$ ratios of the stellar oxide grains are plotted for the four groups defined according to their O-isotopes. Grains without evidence for ^{26}Al are shown as peaks at the left-hand side of the diagram. The distributions are quite different for Groups 1–3 and for the sake of discussion can be viewed as a sequence in the order 3–1–2, with increasing average $^{26}Al/^{27}Al$ ratio and increasing fraction of grains with ^{26}Al (Table 2). The poor statistics for Group 4 grains preclude comparison with the other groups, but it is worth noting that the two Group 4 grains with unambiguous evidence for the presence of ^{26}Al have inferred $^{26}Al/^{27}Al$ ratios similar to the average of Group 1. We also note that the unusual grain T22 (see above) has an inferred $^{26}Al/^{27}Al$ ratio of 1.3×10^{-3}, quite similar to those of the other Group 4 grains, if its ^{26}Mg excess is attributed to the radioactive decay of ^{26}Al.

4. SOURCES OF STELLAR OXIDE GRAINS

The unusual isotopic compositions of the Al_2O_3 and $MgAl_2O_4$ grains described here leave no doubt that these grains are stellar condensates that survived the passage through the interstellar medium and the formation of the solar system. Although they serve as detailed probes of the astrophysical processes occurring in their stellar sources, extracting new information from presolar grains is an iterative process. Current ideas of stellar evolution, based on a combination of existing theory and astronomical observations, are used to infer likely stellar sources for different grains. Precise isotopic measurements of major and minor elements in the grains—made with a dynamic range and accuracy far exceeding that which can be achieved astronomically—are then used to test and refine theoretical models, which leads to a deeper understanding of stellar processes. In this section, we will discuss what types of stars could have produced these unusual dust grains and try to answer the important question: Given that certain grains came from a particular type or types of star, what clues can they provide to further our understanding of how these stars work?

The isotopic signatures of most of the circumstellar oxide grains are characteristic of H burning: ^{17}O enrichments and ^{18}O depletions are the result of the CNO cycles and ^{26}Al is produced by proton captures on ^{25}Mg (Al-Mg chain) (see, e.g., Clayton 1983; Rolfs & Rodney 1988). Although H burning occurs in all stars, the authors of previous discussions of presolar oxide grains have proposed that most grains formed around low- and intermediate-mass ($M = 1$–$8\ M_\odot$) O-rich red giant and asymptotic giant branch (AGB) stars (Hutcheon et al. 1994; Huss et al. 1994a; Nittler et al. 1994, 1995a). This proposition is based on a number of observations:

1. O-rich dust is observed spectroscopically in the atmospheres of O-rich red giants and AGB stars, and such stars are believed to produce the major fraction of O-rich dust in the Galaxy.
2. The O-isotopic compositions of many circumstellar oxide grains from meteorites are similar to those measured spectroscopically in the atmospheres of O-rich red giants and AGB stars.
3. The O-isotopic compositions of most of the grains are quantitatively consistent with the predictions of calculations of evolution, nucleosynthesis, and mixing in red giants.
4. Although O-isotopic measurements are not available for other types of dust-producing stars, such as novae and supernovae, theoretical models predict isotopic compositions for such stars unlike those observed in most of the grains. Moreover, these types of stars probably produce far less O-rich dust than do red giants and AGB stars.

The new data reported here lend further support to the hypothesis of a red giant and AGB star origin for most of the circumstellar oxide grains found to date. We will discuss the arguments in turn, paying particular attention to recent theoretical work on nucleosynthesis and mixing within red giant stars.

4.1. *Observations and Formation of Circumstellar O-rich Dust*

In stellar environments conducive to dust formation, the most important factor governing the composition of condensed solids is the gas phase C to O ratio. For $O > C$, most of the C is locked up in CO molecules, with the excess O being available to combine with other elements to form

oxide grains. Conversely, if C > O, carbonaceous dust forms. This is reflected spectroscopically; C-rich dust-producing stars typically show an 11.2 μm infrared emission feature, characteristic of SiC, while O-rich stars show features at 9.7 and 18.5 μm, associated with stretching and bending modes in silicates. The latter have been observed in both emission and absorption spectra of many circumstellar environments, including O-rich red giants (Treffers & Cohen 1974; Little-Marenin 1986), O-rich planetary nebulae (Aitken et al. 1979), and novae (Bode et al. 1984; Gehrz et al. 1986). In a few exceptional cases, silicate features have also been seen in stars that are optically classified as carbon stars, in apparent conflict with the statement that O-rich dust formation requires an O-rich environment (Little-Marenin 1986; Willems & De Jong 1986). However, these stars are likely transitional objects between O-rich and C-rich stars, and the observed silicate features are thought to be due to preexisting dust shells produced while the stars were O-rich (Willems & De Jong 1986; Kwok & Chan 1993).

Although silicate features are widely observed in circumstellar environments, observational evidence for more refractory oxides like Al_2O_3 and $MgAl_2O_4$ is rare. Nevertheless, thermodynamic calculations of grain condensation predict Al_2O_3 to be the first solid produced upon cooling of an O-rich gas with approximately solar composition. Typical condensation temperatures are in the range $\sim$1400–1700 K, depending on the gas pressure (Lattimer, Schramm, & Grossman 1978; Sharp & Wasserburg 1995; Lodders & Fegley 1995). Some 200–300 K below the condensation point of Al_2O_3, the Al_2O_3 reacts with the gas to form $MgAl_2O_4$. At temperatures slightly lower still, magnesium-rich silicates begin to appear. Onaka, De Jong, & Willems (1989) studied the low-resolution *IRAS* spectra for 109 Mira variable stars and attributed a broad 12 μm feature in many stars to Al_2O_3 grains. They further showed that many of the stars have spectra consistent with circumstellar shells containing mixtures of Al_2O_3 and amorphous silicates and suggested that silicates in circumstellar shells may grow on preexisting Al_2O_3 particles. Note that Al_2O_3 is predicted to condense at some temperature, no matter what the initial C/O ratio. However, for C/O > 1, Al_2O_3 forms by reaction of preexisting AlN with the gas and is stable only over a very small temperature interval (<20–50 K) (Lattimer et al. 1978). Moreover, there is evidence that much of the Al present in C-rich circumstellar shells is locked up in AlN in solid solution in SiC grains, which reduces the amount available to form Al_2O_3 under such conditions (Hoppe et al. 1994a; Hutcheon et al. 1994; Amari et al. 1995a; Lodders & Fegley 1995). We thus conclude that Al_2O_3 is far more likely to form and survive in O-rich environments than in C-rich sites (Lattimer et al. 1978).

Gehrz (1989) has compiled estimates of mass-loss rates, spatial densities, and dust-to-gas ratios for many types of dust-producing stars and inferred that over 90% of dust injected by stars into the interstellar medium comes from low- or intermediate-mass red giants and that some 80% of this dust is O rich. However, this estimate of the relative O-rich rich dust production in red giants may be too high. Jura & Kleinmann (1989) have estimated the numbers of mass-losing O-rich and C-rich AGB stars in the solar neighborhood to be comparable and the O-rich–to–C-rich dust production ratio of AGB stars may thus be closer to 1:1 rather than 8:2. This makes no difference to the relative contribution of AGB stars to the total O-rich dust in the Galaxy, however. Overall, more than 90% of O-rich stardust is expected to come from red giants and AGB stars, with the remainder from red supergiants, supernovae, and novae.

4.2. *Isotopic Measurements of Red Giant Stars*

Spectroscopic determinations of isotopic ratios from atomic spectral lines are extremely difficult owing to the small isotopic shifts of these lines. Molecular lines have much larger relative isotopic shifts, however, and have been widely used to determine isotopic ratios in stars cool enough for molecules to be present, especially red giants and AGB stars (see, e.g., Gustafsson 1989). Figure 9 shows the $^{16}O/^{17}O$ and $^{16}O/^{18}O$ ratios measured spectroscopically in a number of cool giants of various spectral types. Typical error bars ($\sim$25%–50%) are shown for one star of each type. The O-isotopic ratios of all of the stars were determined from molecular lines in the infrared, except for those of the C envelopes, which were determined from radio spectra. Also shown are ellipses indicating the ranges in O-isotopic space spanned by the four groups of circumstellar oxide grains (see Fig. 5).

The K and M stars in Figure 9 are O-rich red giants that have not yet reached the thermally pulsing AGB phase (Harris & Lambert 1984a, 1984b; Harris, Lambert, & Smith 1988). These stars have $^{16}O/^{18}O$ ratios close to the solar ratio and ^{17}O excesses similar to or larger than those observed in Group 1 oxide grains. These ratios are in reasonably good accord with theoretical predictions for red giants. We shall defer a discussion of these theoretical predictions until § 4.3. Following Smith & Lambert (1990), the MS and S stars shown in Figure 9 are divided into two groups, depending on whether or not they show lines of the unstable element technetium, which is produced by the *s*-process in the He-burning shell of AGB stars. Those with Tc are thus O-rich AGB stars; their O-isotopic ratios are quite similar to those of Group 1 grains and are also well explained by standard stellar models. Several of the MS and

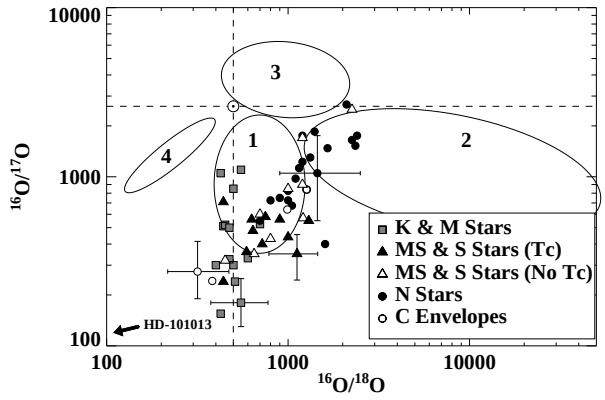

FIG. 9.—O-isotopic ratios measured spectroscopically in different classes of red giant stars; characteristic error bars are shown for one star of each type. Also shown are ellipses indicating ranges of compositions of the four groups of presolar oxide grains. Many of the observed stars have O-isotopic ratios similar to Group 1 oxide grains. Data are from: K and M stars (Harris & Lambert 1984a, 1984b; Harris et al. 1988); MS & S stars (Smith & Lambert 1990); N-type carbon stars (Harris et al. 1987), and dusty C-rich envelopes (Kahane et al. 1992). The arrow in the lower left-hand corner points toward an unusual barium star, HD 101013 (Harris et al. 1985). See text for discussion.

S stars without Tc have $^{16}O/^{17}O$ and $^{16}O/^{18}O$ ratios higher than those observed in the AGB stars with Tc. Smith & Lambert (1990) have proposed that these stars are evolved barium stars; i.e., their surface compositions have been modified by mass transfer from AGB star binary companions and are thus not easily explained by models of evolution of and mixing within single stars. Not shown in Figure 9 are the O-isotopic ratios of six barium stars measured by Harris, Lambert, & Smith (1985). Most of these stars have O-isotopic ratios similar to the K and M stars. One barium star, HD 101013, is quite different from all other observed stars; it is highly enriched in both ^{17}O ($^{16}O/^{17}O = 100$) and ^{18}O ($^{16}O/^{18}O = 60$), relative to their solar abundances.

The N stars shown in Figure 9 are C-rich AGB stars; they have O-isotopic ratios that are systematically higher than those observed in O-rich AGB stars, and their ratios plot in the intermediate region between Group 1 and Group 2 oxide grains (Harris et al. 1987). These ratios are quite difficult to explain by standard models of AGB evolution. The data points designated as C envelopes in Figure 9 represent dusty circumstellar shells around late-type AGB stars (Kahane et al. 1992). Unlike the N stars, they do not appear to have higher $^{16}O/^{17}O$ and $^{16}O/^{18}O$ ratios than O-rich AGB stars. Carbon stars of another type, J stars, are distinguished by very low $^{12}C/^{13}C$ ratios and a lack of the *s*-process element enhancements characteristic of AGB stars. The J stars that have been analyzed for O-isotopic ratios are not shown in Figure 9, but they have $^{16}O/^{17}O$ ratios similar to those of the O-rich AGB stars and several have lower limits on their $^{16}O/^{18}O$ ratios (Harris et al. 1987).

The isotopic ratios of Mg have been analyzed for a number of barium stars and MS and S stars, using MgH lines in the visual spectrum, near 513 nm (Lambert 1991). These studies found ratios identical to the solar ratios within measurement errors, and this result has been used to argue against the $^{22}Ne(\alpha, n)^{25}Mg$ reaction as the source of neutrons for the *s*-process in low-mass AGB stars. Previous attempts to measure $^{26}Al/^{27}Al$ ratios in red giants and AGB stars yielded only upper limits (Lambert 1991), but Guélin et al. (1995) have recently reported the possible detection of the $J = 7$–6 transition line of ^{26}AlF in the millimeter spectrum of the circumstellar envelope IRC +10216. If their identification of this line is correct, their inferred $^{26}Al/^{27}Al$ ratio for this star is 0.037; if not, this ratio is an upper limit. IRC +10216 is the dusty shell around the late-type C-rich AGB star cw Leo and is one of the data points designated as a C envelope in Figure 9.

In summary, there is considerable overlap between the O-isotopic compositions of the circumstellar oxide grains reported here and the compositions of red giants and AGB stars. In particular, many O-rich red giants and most O-rich AGB stars lie within the region occupied by Group 1 grains on an O-isotope plot (Fig. 9). In addition, most C-rich giants (N stars and dusty envelopes around AGB stars) have O-isotopic ratios similar to those of the most ^{18}O-depleted Group 1 grains and the least ^{18}O-depleted Group 2 grains. J stars may have ratios similar to Group 2 grains, since the reported lower limits on their $^{16}O/^{18}O$ ratios indicate they have very little or no ^{18}O. This agreement between the O-isotopic ratios of oxide grains measured in the laboratory, and those obtained from astronomical observations of stars, strongly suggests a red giant or AGB star origin for at least the Group 1 oxide grains. The other groups of oxide grains, particularly Groups 3 and 4, do not have any spectroscopic equivalents, however, but we will argue in § 4.3 that they likely formed in red giants as well. Finally, the $^{26}Al/^{27}Al$ ratio observed in the C-rich envelope IRC +10216, if confirmed, is within a factor of ~2 of the highest inferred $^{26}Al/^{27}Al$ ratio of circumstellar oxide grains from meteorites.

4.3. *Evolution and Nucleosynthesis in Red Giants*

4.3.1. *First and Second Dredge-up*

Most of the lifetime of a star is spent burning hydrogen in its core while on the main sequence. When hydrogen becomes depleted in the core, the star leaves the main sequence and approaches the red giant branch (RGB). As it climbs the RGB, models predict that deep convection mixes the ashes of main-sequence nucleosynthesis into the envelope, changing the surface isotopic and elemental composition. This *first dredge-up* has been extensively studied for several decades now (see, e.g., Iben 1967). Most recently, several theoretical studies have looked in detail at the surface isotopic ratios of the CNO elements following the first dredge-up (Landré et al. 1990; Dearborn 1992; Schaller et al. 1992; Bressan et al. 1993; El Eid 1994; Boothroyd et al. 1994; Mowlavi 1995). El Eid (1994) compared several first dredge-up calculations with each other and found substantial differences in the predicted isotopic ratios between different models owing to variations in stellar parameters such as mass and initial composition and to different treatments of convection as well as different adopted nuclear reaction rates. Nevertheless, some general features are common to all models and conform reasonably well to observations, although these latter are plagued by relatively large uncertainties.

Main-sequence H burning by the CNO cycles destroys essentially all of the ^{18}O that was originally present in the core and results in a layer highly enriched in ^{17}O (^{17}O "pocket"). Consequently, depending on the depth of mixing, following first dredge-up the surface $^{16}O/^{17}O$ ratio can be much lower and the surface $^{16}O/^{18}O$ ratio slightly higher than the initial surface ratios. The predicted $^{16}O/^{17}O$ depends strongly on the star's initial mass. For low-mass stars ($M \lesssim 2.5\ M_\odot$), this dependence results primarily from the increase of the depth of dredge-up with stellar mass. Mixing in a 1 $M_\odot$ star barely reaches the ^{17}O pocket and the surface retains its initial $^{16}O/^{17}O$ ratio, whereas enough of the ^{17}O pocket is mixed into the envelope of a 2.5 $M_\odot$ star to decrease the ratio to ~200. For higher mass stars, the entire ^{17}O pocket is dredged up, but since more ^{17}O is destroyed at the H-burning temperatures of these stars, the peak concentration in the ^{17}O pocket is smaller and the surface is not as highly enriched in ^{17}O as for 2.5 $M_\odot$ stars. Published predictions of $^{16}O/^{17}O$ ratios in the mass range $M \approx 2.5$–10 $M_\odot$ are highly variable, owing to large uncertainties in the $^{17}O(p, \alpha)^{14}N$ and $^{17}O(p, \gamma)^{18}F$ reaction rates at stellar temperatures. However, a direct measurement of the $^{17}O(p, \alpha)$ cross section at stellar energies with much reduced uncertainties has recently been reported (Blackmon et al. 1995). The new rate is close to the minimum value allowed by the measurements of Landré et al. (1990) and first dredge-up calculations using the new rate predict $^{16}O/^{17}O$ ratios similar to those of previous calculations that used the Landré et al. (1990) rate (M. F. El Eid, private communication). Comparisons of dredge-up models with observations of K and M stars have previously led

Boothroyd et al. (1994) to the same conclusion, namely that the true $^{17}O(p, \alpha)^{14}N$ rate is close to the rate of Landré et al. (1990). Models using this rate predict surface $^{16}O/^{17}O$ ratios that increase with solar mass from the minimum value of ~ 200 for a 2.5 $M_\odot$ star to ~ 800 for a 10 $M_\odot$ star (Boothroyd & Sackmann 1997).

As stated above, because the material mixed into the envelope is depleted in ^{18}O, the surface $^{16}O/^{18}O$ ratio is expected to increase after the first dredge-up. However, because the proportion of ^{18}O-depleted material mixed into the envelope is relatively small, the predicted change in the surface $^{16}O/^{18}O$ ratio is much smaller and depends much less steeply on stellar mass than the change in the $^{16}O/^{17}O$ ratio. Again, the predicted ratio depends on a poorly known nuclear reaction rate, in this case that governing the reaction $^{18}O(p, \alpha)^{15}N$, and observations of red giants have been used to argue that this rate is close to its lowest experimentally allowed value (Harris & Lambert 1984b; Dearborn 1992; Boothroyd et al. 1994). Models using the preferred ^{18}O destruction rate predict a change of $\sim 10\%$–50% in the surface $^{16}O/^{18}O$ ratio after first dredge-up for stars from 1 to 15 $M_\odot$ (Dearborn 1992; El Eid 1994; Boothroyd et al. 1994).

The RGB phase ends with the initiation of a core He-burning phase, and the star shrinks. Following exhaustion of He in the stellar core, the star again ascends the giant branch, this time as a thermally pulsing asymptotic giant branch (TP-AGB) star. For stars of mass $M \gtrsim 3\ M_\odot$, this phase begins with another deepening of the convective envelope, mixing more nuclear-processed material to the surface, the *second dredge-up*. For metallicities close to solar, the second dredge-up is not expected to change the surface O-isotopic ratios substantially from their first dredge-up values (El Eid 1994; Boothroyd & Sackmann 1997). This is not true for stars of lower metallicity, since such stars experience shallower (or no) first dredge-up, but the second dredge-up in these stars is predicted to produce surface O-isotopic ratios similar to those obtained from the first dredge-up in higher metallicity stars. Thus, stars at the beginning of the TP-AGB phase are expected to have surface O-isotopic ratios as described above for the first dredge-up. A possible exception was found for 7 $M_\odot$ stars in the models of Boothroyd & Sackmann (1997). The second dredge-up in these models reached layers that were enriched in ^{18}O from partial He-burning, which led to decreased surface $^{16}O/^{18}O$ ratios. Because this has not yet been seen in other models and since 7 $M_\odot$ stars, owing to their relatively low abundance, are unlikely to have contributed a significant fraction of the presolar oxide grains reported here, this effect will not be discussed further.

Figure 10 shows predictions by Boothroyd & Sackmann (1997) for the surface O-isotopic ratios of different stars following the first and second dredge-ups, along with the data for oxide grains. In this plot, each open circle represents a different star of a given mass and metallicity. The O-isotopic trends described above are apparent. For stars of mass $\lesssim 2.5\ M_\odot$, the $^{16}O/^{17}O$ ratio is a strong function of stellar mass and, for stars of mass $\gtrsim 1.4\ M_\odot$, is largely independent of its initial value. For a given metallicity, the $^{16}O/^{18}O$ ratio varies little with mass, and variations larger than $\sim 50\%$ must be due to differences in initial O-isotopic composition, as originally pointed out by Boothroyd et al. (1994). The most likely cause of variations in initial composition is the chemical evolution of the

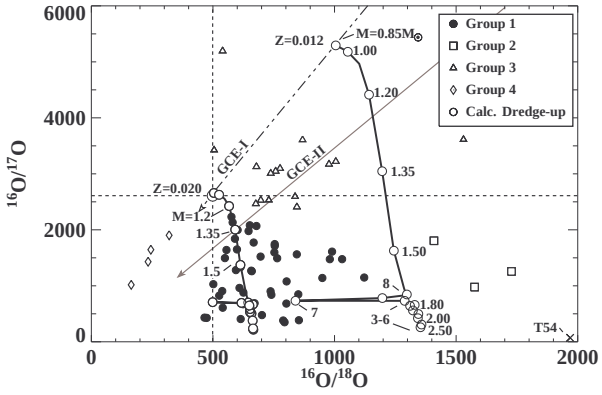

FIG. 10.—Comparison of oxide grain data with predictions of O-isotopic ratios following first and second dredge-up in red giant stars (Boothroyd & Sackmann 1997). For the sake of clarity, error bars on grain measurements are not shown here or in subsequent figures. Each open circle represents a distinct star of different mass and one of two initial compositions, or metallicities. Two possible trends for the Galactic evolution of O-isotopes are also shown; "GCE-I" was used to relate stellar composition to metallicity in the dredge-up models, and "GCE-II' is the trend implied by observations of molecular clouds throughout the galaxy (see § 5). The predicted post–dredge-up $^{16}O/^{17}O$ ratio depends strongly on stellar mass, whereas the $^{16}O/^{18}O$ ratio changes little from its initial value. The Group 1 and 3 oxide grains have isotopic compositions consistent with these predictions, provided they come from several different stars with distinct masses and initial compositions. See text for further discussion.

Galaxy. For the two dredge-up curves shown in Figure 10, Boothroyd & Sackmann (1997) assumed initial O-isotopic ratios that are inversely proportional to stellar metallicity (double-dot–dashed line labeled "GCE-I" in Fig. 10), following the chemical evolution model of Timmes, Woosley, & Weaver (1995). The gray line labeled "GCE-II" in Figure 10 represents the Galactic chemical evolution trend implied by radio observations of molecular clouds throughout the Galaxy; this trend may be more representative of the O-isotopic evolution of the average interstellar medium than the evolution line used for the first dredge-up calculations of Boothroyd and Sackmann (see § 5).

It is clear from Figure 10 that the O-isotopic ratios of the Group 1 oxide grains are well explained by first dredge-up in red giant stars, provided the grains come from several different stars with distinct masses and initial O-isotopic ratios. It is apparent as well that the O-isotopic compositions of Group 3 grains probably also reflect an origin in red giant stars. However, if this is the case, their stellar sources must have had initial $^{16}O/^{17}O$ and $^{16}O/^{18}O$ ratios higher than the solar values and masses low enough ($\lesssim 1.4\ M_\odot$) that they did not dredge up enough ^{17}O to substantially lower their high initial $^{16}O/^{17}O$ ratios. It is likely that the Group 3 grains largely retain the original O-isotopic ratios of their parent stars and thus provide important information about the Galactic evolution of O-isotopic ratios. The issue of Galactic chemical evolution and its implications for presolar oxide grains are discussed in more detail in § 5.

4.3.2. *Third Dredge-up in TP-AGB Stars*

Stars in the TP-AGB phase of their evolution consist of an electron-degenerate C-O core surrounded by thin He-burning and H-burning shells and a large convective envelope. They undergo periodic He-shell flashes (thermal pulses) in which the He shell burns very strongly, temporarily extinguishing the overlying H shell. Subsequent con-

vection mixes material processed in the two burning shells into the convective envelope; these convective episodes are collectively referred to as the third dredge-up (see, e.g., Iben & Renzini 1983). The dredged-up material is primarily ^{4}He and ^{12}C but also includes the products of *s*-process neutron capture nucleosynthesis and, of primary importance here, ^{26}Al produced in the H shell by the Mg-Al chain. Forestini, Paulus, & Arnould (1991) obtained a surface ^{26}Al/^{27}Al ratio of 1.5×10^{-3} from third dredge-up in a 3 $M_\odot$ AGB star. Other models give similar ratios, in the range 10^{-3}–8×10^{-2} (Gallino et al. 1994; Guélin et al. 1995; Wasserburg et al. 1994).

Most of the presolar oxide grains that show evidence for the prior presence of ^{26}Al have inferred ^{26}Al/^{27}Al ratios in the range of theoretical predictions for AGB stars, which strengthens the argument that many of the grains originated in such sites. However, the grains whose O-isotopic ratios reflect the first dredge-up but that do not have ^{26}Al must have formed either in red giants before the TP-AGB phase or in AGB stars that did not experience enough third dredge-up episodes to bring appreciable amounts of ^{26}Al to the surface. Note that dust production is strongly related to mass-loss rates, which are highest during the late stages on the AGB. Low-mass ($M \lesssim 1.2\ M_\odot$) stars are predicted to lose most of their mass while on the RGB, before reaching the AGB, whereas higher mass stars lose little mass before the onset of thermal pulses (Boothroyd & Sackmann 1988). Since a low-mass star thus begins the TP-AGB phase with a much diminished envelope mass, its entire envelope may be lost after only a few thermal pulses, before any third dredge-up convective episodes occur. That the occurrence of third dredge-up depends strongly on the mass of an AGB star is supported by the calculations of R. Gallino et al. (private communication), who self-consistently predict third dredge-up in a 1.5 $M_\odot$ AGB star, but not in a 1 $M_\odot$ star. Group 3 grains have O-isotopic ratios that reflect first dredge-up in low-mass stars ($M \lesssim 1.4\ M_\odot$; see above). Based on the above discussion, it is expected that a large fraction of these grains formed in stars that did not experience the third dredge-up, which is consistent with the observation that a much smaller fraction of Group 3 grains has ^{26}Al, compared to Group 1 grains, which probably formed in stars of higher mass. An alternative source for some of the grains without ^{26}Al is planetary nebulae (PNs), after the ^{26}Al dredged up on the AGB has decayed. However, since it is not certain that any of the dust observed in planetary nebulae actually formed during the PN stage (Whittet 1992), this scenario is less likely (see § 4.4).

The highest predicted ^{26}Al/^{27}Al ratios ($\gtrsim 10^{-2}$) obtained by dredge-up of H-shell material are reached only after many thermal pulses and with extensive loss of the stellar envelope by winds. AGB stars at these late stages are expected to have become carbon stars from the dredge-up of ^{12}C and thus to produce carbonaceous dust instead of oxides. That the apparent ^{26}Al/^{27}Al ratio of 0.04 observed in IRC +10216, the dusty shell around the very late stage C star cw Leo (§ 4.2), is higher than the inferred ratio in any of the Al_2O_3 grains is consistent with this, since the oxide grains presumably formed before their parent stars became C-rich. However, in this regard, it is somewhat of a surprise that the bulk of meteoritic presolar SiC grains, which probably come from C-rich AGB stars, have inferred ^{26}Al/^{27}Al ratios quite similar to those of the oxide grains and not significantly higher ratios (Hoppe et al. 1994a).

Since the presence of ^{26}Al in many presolar oxide grains indicates that they formed around TP-AGB stars, we must address the issue of the effect of the third dredge-up on their surface O-isotopic ratios. Only small changes from the first and second dredge-up values are expected if the amount of the three oxygen isotopes mixed into the envelope is small relative to the total amount of O in the envelope. This is probably the case for ^{16}O and ^{17}O, and the third dredge-up is unlikely to change the surface ^{16}O/^{17}O ratios by more than $\sim$10% (Boothroyd et al. 1994; A. Boothroyd, private communication). The situation for ^{16}O/^{18}O is more complicated, however. Oxygen-18 is both created [by the reactions ^{14}N(α, γ)^{18}F(e^+, ν)^{18}O] and destroyed [by ^{18}O(α, γ)^{22}Ne] during He burning. Early thermal pulses could thus produce large amounts of ^{18}O, which could be dredged up before it is destroyed in later pulses (Boothroyd & Sackmann 1988; Boothroyd et al. 1994; N. Mowlavi, private communication). Observations of AGB stars that have experienced some third dredge-up episodes (MS and S stars with Tc and other *s*-process elements; § 4.2) do not show large ^{18}O excesses. The O-isotopic ratios in these stars are similar to the first dredge-up values seen in K and M giants, which suggests that the third dredge-up indeed has little effect on the surface O-isotopic compositions of most AGB stars. A similar conclusion is indicated by the Group 1 oxide grains, since these have O-isotopic ratios that are well explained by theoretical predictions of first and second dredge-up, even though ^{26}Mg excesses show that most of the grains formed in stars that must have experienced third dredge-up. Moreover, there is no correlation between inferred ^{26}Al/^{27}Al ratios and O-isotopic ratios for Group 1 grains.

Although a large decrease in the surface ^{16}O/^{18}O ratio from the third dredge-up after early thermal pulses is apparently ruled out for *most* AGB stars, Harris, Lambert, & Smith (1985) proposed this mechanism to explain the low ^{16}O/^{18}O ratio observed in the barium star HD 101013 (§ 4.2). Dredge-up of ^{18}O after early thermal pulses may also account for the ^{18}O excesses observed in Group 4 oxide grains. These grains have inferred ^{26}Al/^{27}Al ratios in the range expected for third dredge-up of H-shell material and ^{16}O/^{17}O ratios consistent with first dredge-up in low-mass stars ($M \lesssim 1.5\ M_\odot$). In addition, the ^{25}Mg and ^{26}Mg excesses observed in the Group 4 grain T22 are consistent with predictions of *n*-capture in the He shell followed by third dredge-up. So far, no model has self-consistently predicted dredge-up of ^{18}O from the He shell, and the calculations are hampered by large uncertainties in the ^{18}O(α, γ)^{22}Ne reaction rate (Wiescher et al. 1993). The possibility that the low ^{16}O/^{18}O ratios in Group 4 grains reflect such dredge-up, however, accentuates the need for further detailed modeling to determine whether this is a viable scenario. An alternative explanation for the ^{18}O excesses in Group 4 grains is Galactic chemical evolution and is discussed further in § 5.

4.3.3. *Hot Bottom Burning*

We address now the Group 2 circumstellar oxide grains. An origin in AGB stars for Group 2 grains is suggested by their inferred ^{26}Al/^{27}Al ratios, which are in the range predicted for TP-AGB stars, and their ^{16}O/^{17}O ratios, which are similar to those of many Group 1 grains. However, the degree of ^{18}O depletion observed in these grains is much larger than can be explained by the admixture of nuclear-

processed material into the stellar envelope by the dredge-up processes discussed thus far. One proposed mechanism for lowering the ^{18}O abundance at the surface of relatively high mass TP-AGB stars ($M \approx 4$–$7\ M_\odot$) is "hot bottom burning" (HBB), where the base of the convective envelope becomes hot enough for H-burning reactions to occur (Sugimoto 1971; Cameron & Fowler 1971). Because it is fully convective, the entire envelope is cycled through the hot region at its base, so that the products of CNO-cycle nucleosynthesis are enriched at the stellar surface. Boothroyd et al. (1995) have calculated the effects of HBB on O-isotopic ratios and shown that for stars of 4.5–7 $M_\odot$, HBB rapidly destroys essentially all of the envelope's ^{18}O and then gradually converts ^{16}O to ^{17}O, which decreases the $^{16}O/^{17}O$ ratio from its second dredge-up value. The predicted surface isotopic ratios depend on many parameters, in particular on uncertain reaction rates and mass-loss rates. Nevertheless, these authors came to two important conclusions with regard to circumstellar oxide grains. The first conclusion is that the ^{18}O destruction is complete and rapid, which rules out HBB as an explanation for the large but not total ^{18}O depletions observed in several Group 2 grains ($^{16}O/^{18}O \sim 1000$–4000). Although the intermediate ^{18}O depletions observed in some of these grains may be due to contribution of background O on the sample mounts to the isotopic measurements, for some of the larger grains this can be ruled out. The second conclusion is that the maximum final $^{16}O/^{17}O$ ratio resulting from HBB is ~ 1000 for a 7 $M_\odot$ star, and this only with the highest ^{17}O destruction rates allowed by the Landré et al. (1990) compilation. However, the $^{17}O(p, \alpha)^{14}N$ and $^{17}O(p, \gamma)^{18}F$ rates have recently been shown to be close to the minimum Landré et al. (1990) values (Blackmon et al. 1995), and the maximum HBB $^{16}O/^{17}O$ ratio with these new rates is ~ 600 (Boothroyd et al. 1995). Because most Group 2 oxide grains have $^{16}O/^{17}O$ ratios higher than this, indicating that they formed in low-mass ($M \lesssim 2\ M_\odot$) stars, HBB is apparently ruled out as an explanation for the compositions of these grains. This is not surprising since stars of mass greater than 4 $M_\odot$ are much less common than stars of lower mass and thus less likely to have contributed much dust to the solar system. Note that, although HBB is also expected to produce ^{26}Al, inferred $^{26}Al/^{27}Al$ ratios of oxide grains are much less diagnostic than the O-isotopic ratios since $^{26}Al/^{27}Al$ ratios predicted by HBB models are similar to those expected from dredge-up of H-shell material (Nørgaard 1980; Cameron 1993; Frost & Lattanzio 1996).

Although hot bottom burning AGB stars are thus an unlikely source for Group 2 grains, HBB may have produced the composition of the highly ^{17}O-enriched grain T54 ($^{18}O/^{16}O \lesssim 0.0005$; $^{17}O/^{16}O = 0.014$). If this grain's true $^{18}O/^{16}O$ ratio is much lower than its measured value, as suggested above, its composition is similar to the predictions of Boothroyd et al. (1995) for the final composition of a HBB 7 $M_\odot$ star ($^{18}O/^{16}O \approx 0$; $^{17}O/^{16}O \approx 0.009$). The discovery of additional grains like T54 could potentially provide important constraints on HBB in AGB stars.

4.3.4. *Cool Bottom Processing*

The fact that hot bottom burning cannot quantitatively explain the ^{18}O depletions observed in Group 2 circumstellar oxide grains led Boothroyd et al. (1995) to propose that some form of extra mixing might occur in low-mass AGB stars, called "cool bottom processing" (CBP) by these authors. The conjecture is that this process would transport material from the convective envelope to regions hot enough for some H-burning reactions to occur and then transport it back to the envelope. Extra mixing has also been proposed to explain low $^{12}C/^{13}C$ ratios in low-mass stars on the RGB (Gilroy 1989; Gilroy & Brown 1991; Charbonnel 1994, 1995). A plausible physical mechanism for such deep mixing is the interaction between rotation-induced turbulence and meridional circulations (Zahn 1992; Charbonnel 1994). To explore the effects of CBP on the CNO isotopes in low-mass red giants, Wasserburg et al. (1995) computed parameterized models and determined that both the observed $^{12}C/^{13}C$ ratios in red giants and the O-isotopic ratios in Group 2 oxide grains (and N-type C stars) could be reproduced with identical model parameters (essentially the difference in temperature between the base of the extra mixing and the H-burning shell). The isotopic compositions resulting from CBP were found to depend primarily on the temperature in the zone reached by the mixing, not on the details of the mixing process itself. In these models, CBP on the RGB reached layers with high enough temperatures to reduce the $^{12}C/^{13}C$ ratio of the envelope to a low value, but the oxygen isotopes were modified only at the higher temperatures reached by deep mixing on the AGB.

The predicted effects (Wasserburg et al. 1995) of cool bottom processing on the O-isotopic ratios of AGB stars of mass 1, 1.5, and 1.65 $M_\odot$ and solar metallicity are shown in Figure 11. The $^{16}O/^{18}O$ ratio was found to increase exponentially with time on the AGB and the $^{16}O/^{17}O$ ratio to decrease gradually. Clearly, these results need to be confirmed by full stellar evolutionary calculations, including both third dredge-up and some physical model of deep mixing. Nevertheless, the good agreement between these parametric models and the compositions of Group 2 grains, as well as the generic nature of the mixing calculation, supports the suggestion that some sort of CPB is indeed responsible for the ^{18}O depletions in these grains. The high inferred $^{26}Al/^{27}Al$ ratios of Group 2 grains are consistent

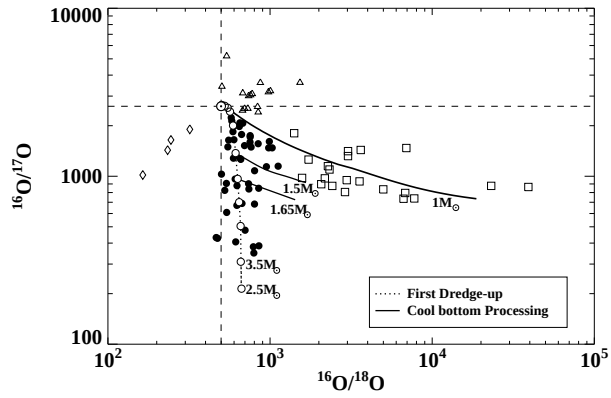

FIG. 11.—Comparison of O-isotopic ratios in presolar oxide grains with those predicted from cool bottom processing, deep extra mixing in low-mass AGB stars (Wasserburg et al. 1995). Grain symbols are the same as in previous figures, and the first dredge-up curve (*dotted line*) is the same as the $Z = 0.02$ curve shown in Fig. 10. Cool bottom processing increases the $^{16}O/^{18}O$ ratio from its first dredge-up value and decreases the $^{16}O/^{17}O$ ratio. The good agreement of this model with the Group 2 grain data suggests that extra mixing is indeed responsible for the ^{18}O depletions in these grains. These data further imply that cool bottom processing occurs only in stars of lower mass than $\sim 1.5\ M_\odot$.

with such a scenario as well, since thermal pulses and third dredge-up of ^{26}Al should occur along with the CBP.

Cool bottom processing can only occur if there is no discontinuity in the mean molecular weight to prevent it (Charbonnel 1994). For example, a large composition (and thus, molecular weight) discontinuity is left behind after deepest convection during first dredge-up but is soon erased by the advancing H-burning shell. Based on the presence or lack of such molecular weight discontinuities at different stages of evolution for different stars, Boothroyd & Sackmann (1997) have estimated that CBP can occur throughout the TP-AGB phase for stars of mass $\lesssim 3.5\ M_\odot$. However, the circumstellar oxide grain data suggest that the mass range over which CBP sufficient to change the O-isotopic ratios occurs is narrower. As seen in Figure 11, all of the Group 2 grain oxygen data can be explained by CBP in stars with masses less than $\sim 1.5\ M_\odot$. In fact, since CBP is expected to decrease the surface $^{16}O/^{17}O$ ratio from its first dredge-up value, the first dredge-up predictions described above show that CBP in stars of mass 2–3.5 $M_\odot$ will result in substantial ^{18}O depletions and in $^{16}O/^{17}O$ ratios in the range $\sim$200–500. Because no grains with such compositions have been found, we propose that if cool bottom processing does, in fact, occur in AGB stars in the 2–3.5 $M_\odot$ mass range, it does so without altering the surface O-isotopic ratios of the stars. This is unlikely to be due to lack of grains from stars in this mass range, since the compositions of some Group 1 grains are adequately explained by first dredge-up in such stars and CBP would destroy the accord.

4.4. *Other Possible Sources of Stellar Oxide Grains*

In addition to low- and intermediate-mass red giants and AGB stars, Gehrz (1989) includes planetary nebulae, red supergiants, supernovae, Wolf-Rayet stars, and novae in his inventory of stellar types that produce O-rich dust. Except for planetary nebulae, which likely do not produce dust (Whittet 1992), all of these must be considered as potential sources of presolar oxide grains. Massive stars (red supergiants, supernovae of Type II, and Wolf-Rayet stars) are estimated to produce 5%–10% of O-rich stardust in the ISM (Gehrz 1989; Whittet 1992). O-rich dust is observed to condense in red supergiants, and these stars are expected to mix the products of core and shell H burning into their envelopes in dredge-up episodes, just as do their lower-mass cousins described in previous sections. Two M supergiants, α Ori and α Sco, are among the K and M stars whose data are plotted in Figure 9, and their O-isotopic ratios clearly reflect the first dredge-up (Harris & Lambert 1984a). For solar metallicity stars of mass 9–25 $M_\odot$, the first dredge-up models of Schaller et al. (1992) predict $^{16}O/^{17}O$ ratios of $\sim$900–1200 and $^{16}O/^{18}O$ ratios $\sim$20% higher than the initial values. These authors used a value for the $^{17}O(p, \alpha)^{14}N$ reaction rate about 70% higher than the (more precise) Blackmon et al. (1995) rate, however, and thus probably overestimated the $^{16}O/^{17}O$ ratio. Using the Blackmon et al. (1995) rate, M. F. El Eid (private communication) predicts $^{16}O/^{17}O$ ratios of $\sim$600–1100 for stars of mass 11–15 $M_\odot$. We take this range as being representative of supergiants following first dredge-up. Although stars with $M \gtrsim 10\ M_\odot$ do not experience thermal pulses, ^{26}Al produced during shell H burning is expected to be mixed to the surface of these stars. Woosley & Weaver (1995) predict $^{26}Al/^{27}Al$ ratios in the range 1.7×10^{-4}–2.0×10^{-2} in the H envelope of stars of mass 13–25 $M_\odot$, similar to the range predicted for AGB stars and observed in the oxide grains. Approximately one-fourth of the circumstellar oxide grains have $^{16}O/^{17}O$ ratios in the range 600–1100, $^{16}O/^{18}O$ ratios in the range 500–1000, and varying $^{26}Al/^{27}Al$ ratios; red supergiants should be considered a potential source of these Group 1 grains.

Some meteoritic grains of SiC, graphite, and Si_3N_4 have isotopic compositions indicating that they formed in Type II supernovae (SNs) (Amari et al. 1992; Nittler et al. 1995b, 1996). However, much more oxygen is ejected in SN explosions than carbon. For example, Woosley & Weaver (1995) predict O/C = 2–8 for the ejecta of SNs of mass 11–25 $M_\odot$, which leads one to expect to find O-rich SN condensates in meteorites in addition to the C-rich grains already found. Dust formation has been confirmed observationally in SN 1987A both by increased infrared flux and shifts of optical emission lines (see, e.g., Colgan et al. 1994) and Al_2O_3 may be an important constituent of this dust (Kozasa, Hasegawa, & Nomoto 1991). Before a massive star explodes as a supernova, it is believed to have more or less an "onionskin" structure, which consists of concentric zones with different chemical and isotopic compositions due to different nuclear-burning histories. Astronomical observations, hydrodynamic models, and the isotopic compositions of C-rich SN dust in meteorites all show that significant, but selective, mixing between the zones must occur in the ejecta (Shigeyama & Nomoto 1990; Herant & Woosley 1994; Nittler et al. 1996).

Most oxide grains from SNs would form from material in O-rich shells (He-, C-, and Ne-burning zones). Although the O-isotopic ratios of SN grains will depend on the extent of mixing as well as the initial mass of the pre-SN star, these zones will produce grains highly enriched in ^{16}O. Such grains would plot in the extreme upper right-hand corner of Figure 5; no oxide grains with this isotopic signature have been found, and there is thus no evidence for SN grains in the current data set. Note that, in principle, grains could condense in the hydrogen envelope unmixed with other zones; these would have O-isotopic ratios similar to red supergiants. However, the O in the envelope constitutes only a small fraction ($\lesssim$12%; Woosley & Weaver 1995) of the total oxygen in the ejecta, and most grains should be very ^{16}O-rich. Moreover, the lack of shifts in hydrogen emission lines with the onset of dust formation in SN 1987A suggests that dust condenses primarily in the inner, ^{16}O-rich regions of the ejecta (Colgan et al. 1994).

Wolf-Rayet (WR) stars are very massive stars ($M > 25\ M_\odot$) in which extreme mass loss by stellar winds has stripped off the outer layers, exposing the products of H and He burning at the surface. They have O > C in the so-called Of and WN phases and could, in principle, produce oxide grains during these stages. Note, however, that dust formation in WR stars has been confirmed observationally only in the late, C-rich, WC phase of evolution and not during the Of and WN phases (Gehrz 1989). Nevertheless, during these stages, the products of core CNO-cycle nucleosynthesis appear at the surface of the stars. This would result in O-isotopic ratios similar to those predicted for extreme hot bottom burning in AGB stars (see § 4.3) (Boothroyd et al. 1995), namely $^{16}O/^{18}O \approx \infty$, and very low $^{16}O/^{17}O$ ratios ($^{16}O/^{17}O \lesssim 100$) (see Prantzos et al. 1986). As described above, Al_2O_3 grain T54 is the only grain that has such an isotopic signature. If the true

$^{16}O/^{18}O$ ratio of T54 is close to infinity, then a Wolf-Rayet star origin for this grain is possible.

Novae and supernovae of Type Ia are both believed to result from the accretion of matter from a binary companion onto a white dwarf, followed by a thermonuclear runaway. In the former case, it is the accreted matter that explodes; in the latter, the entire star is disrupted. Nucleosynthesis in novae is characterized by hydrogen burning at high temperatures, where the energy generation is mainly from the hot CNO cycles (Woosley 1986). Hot CNO-cycle burning usually produces C > O, and in most cases where dust has been observed around novae, it is C-rich (Gehrz 1988). The observation of infrared features associated with silicates in a few novae (Bode et al. 1984; Gehrz et al. 1986) indicates the possibility that oxide grains form in such explosions. However, hot CNO cycle burning in novae is predicted to produce very large excesses of ^{17}O and ^{18}O, relative to ^{16}O and solar, with $^{16}O/^{17}O$ and $^{16}O/^{18}O$ typically $\lesssim 10$–20 (Woosley 1986; Politano et al. 1995). None of the oxide grains considered here have these compositions and novae are thus highly unlikely to have produced any of them. Nucleosynthesis in Type Ia supernovae is predicted to produce very high $^{16}O/^{17}O$ and $^{16}O/^{18}O$ ratios ($>10^9$) (Thielemann, Nomoto, & Yokoi 1986), and so these stars also can be ruled out as sources for the bulk of the circumstellar oxide grains.

5. GALACTIC CHEMICAL EVOLUTION AND CIRCUMSTELLAR OXIDE GRAINS

As we have shown in § 4.3, the O-isotopic ratios of Group 1 and Group 3 circumstellar oxide grains are consistent with predictions for the first dredge-up in red giants, provided the stars that produced the grains had a range of initial O-isotopic compositions. One plausible explanation for such variations is the chemical evolution of the Galaxy: as the Galaxy evolves, new generations of stars are born and die, returning freshly synthesized nuclei to the interstellar medium (ISM). In this way, the abundances of the heavy elements have increased throughout the history of the Galaxy, and stars formed at different times (and places) have, *on average*, different chemical and isotopic compositions. Since ^{16}O can be synthesized in a star of initially pure H and He, it is considered a "primary" nucleosynthesis product, whose abundance increases linearly with metallicity, Z. On the other hand, ^{17}O and ^{18}O require preexisting CNO nuclei for their synthesis (the former by $^{16}O + p$; the latter by $^{14}N + \alpha$) and are termed "secondary" nuclei; their abundances should increase as Z^2(Clayton 1988). One may thus, as a first approximation, assume that the average ISM $^{17}O/^{16}O$ and $^{18}O/^{16}O$ ratios increase linearly with metallicity. Furthermore, if the average metallicity of the Galaxy increases monotonically with time, these ratios should be lower in older stars than in younger ones.

These ideas are supported both by radio observations of O-isotopic ratios in molecular clouds throughout the Galaxy and by the circumstellar oxide grain data. The former show a remarkable uniformity of the $^{18}O/^{17}O$ ratio (≈ 3.5) and negative gradients of $^{17}O/^{16}O$ and $^{18}O/^{16}O$ with galactocentric radius (Penzias 1981; Wilson & Rood 1994; Henkel et al. 1995). Such behavior is expected if ^{16}O is primary and ^{17}O and ^{18}O are both purely secondary as described above. (The well-known problem of fitting the solar abundances into this scenario is described below.) The low $^{17}O/^{16}O$ ratios of Group 3 oxide grains (Fig. 6) indicate both that these grains formed in low-mass ($<1.4\ M_\odot$) stars and that these stars had lower than solar initial $^{17}O/^{16}O$ ratios. The latter point can be easily understood in terms of chemical evolution. Due to their longer evolutionary timescales, the low-mass stars that produced Group 3 grains probably formed at an earlier time than the higher mass progenitors of Group 1 grains and thus formed, on average, from less-processed material.

To explore these ideas in more depth, we combine chemical evolution and dredge-up models to predict average O-isotopic ratios for a set of stars of mass 1.1–3 $M_\odot$, a likely range for stars that provided grains to the solar system. We let $\tau(M, Z)$ be the lifetime of a star of mass M and metallicity Z, as given by Mathews, Bazan, & Cowan (1992), and $T_G(Z)$ be the age of the Galaxy when the average metallicity had grown to the value Z, determined from the Galactic evolution age-metallicity relation of Timmes et al. (1995). Then, for each star of mass M, the metallicity Z is chosen to satisfy the equation

$$\tau(M, Z) + T_G(Z) = T_\odot, \tag{3}$$

where $T_\odot$ is the age of the Galaxy at the time of solar system formation, here taken to be 10.5 Gyr. The first–dredge-up O-isotopic ratios for the resulting set of masses and metallicities, as well as for the same set of masses, but somewhat higher and lower metallicities, were interpolated (or extrapolated, if necessary) from the calculations of Boothroyd & Sackmann (1997). These authors, following Timmes et al. (1995), assumed that the initial $^{16}O/^{17}O$ and $^{16}O/^{18}O$ ratios of stars vary in inverse proportion to [Fe/H], which they relate simply to Z (Boothroyd & Sackmann 1997). This evolution trend is indicated in Figure 10 by the dashed line labeled "GCE-I."

Results of our model are shown in Figure 12, overlaid on the Group 1 and 3 oxide data. The theoretical trends are plotted as follows: crosses connected by a solid line for the "average" trend; long-dashed lines for 25% higher (left)

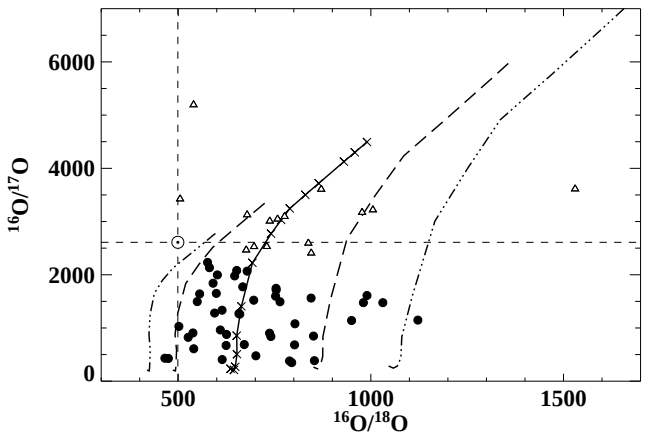

FIG. 12.—Comparison of circumstellar oxide grains (symbols are the same as in previous figures) with the results of a simple Galactic chemical evolution model. The central theoretical trend (crosses connected by a thick line) represents a series of stars of mass 1.1 $M_\odot$ (*top of curve*) to 3 $M_\odot$ (*bottom of curve*) and metallicities chosen from stellar lifetime and chemical evolution models such that they ended their life at the time of solar system formation (see text). The tracks to the right and left represent the same set of masses, but with 25% (*long-dashed lines*) and 45% (*triple-dot-dashed lines*) lower and higher metallicities, respectively, compared to the central "average" trend. The good agreement shows that chemical evolution plays an essential role in establishing the O-isotopic compositions of Group 1 and 3 oxide grains although there must have been a spread about the average metallicities for stars that provided O-rich dust to the solar system.

and 25% lower (right) metallicity; and triple-dot–dashed lines for 45% higher (left) and 45% lower (right) metallicity. Each point along the central track represents the predicted average O-isotopic composition of stars of a given mass that ended their lives at the time of solar system formation; this trend passes through the centers of the Group 1 and 3 O-isotopic distributions. The surprisingly good agreement between this simple model and the distribution in O-isotopic space of Group 1 and Group 3 oxide grains strengthens the conclusion that these grains did indeed form in red giants and that Galactic chemical evolution plays an essential role in determining the isotopic compositions of the grains. Edvardsson et al. (1993) have determined elemental abundances in 189 field disk dwarfs and found that, although the average metallicity in the Galaxy has increased with time, there is considerable variation in the metallicities of stars born at any given time. These authors estimate a spread about the mean of approximately $\pm 45\%$ in Z for stars that formed at the same time and same galactocentric radius as the Sun. As can be seen in Figure 12, a spread of $\pm 45\%$ (outermost theoretical trends) in metallicity is consistent with the range of O-isotopic ratios of Group 1 and 3 grains. However, most of the Group 1 and 3 data lie within the curves that correspond to a smaller range of $\pm 25\%$. In fact, the five Group 1 grains that fall outside this range have $^{16}O/^{17}O$ ratios similar to Group 2 grains and may belong to them (see Fig. 5).

Although the O-isotopic ratios observed in molecular clouds throughout the Galaxy can be understood in terms of the expected primary/secondary/secondary production of $^{16}O/^{17}O/^{18}O$, the measured ratios of the solar system do not fit easily into this picture (Kahane et al. 1992; Wilson & Rood 1994). In particular, the $^{18}O/^{17}O$ ratio of the Sun is 5.2, whereas the interstellar medium has the much lower ratio of 3.5, regardless of galactocentric radius. Furthermore, the current local ISM $^{16}O/^{18}O$ ratio is 560 ± 25 (Wilson & Rood 1994), higher than the solar value of 499. This is difficult to understand; the simple picture of chemical evolution discussed above predicts a substantially lower value in the present ISM than in the solar system, since the ^{18}O abundance is expected to have built up more than ^{16}O in the 4.6 billion years since solar system formation. From their Galactic chemical evolution study, Edvardsson et al. (1993) concluded that the Sun is a "typical" star for its age, metallicity, and Galactic orbit. This does not preclude isotopic peculiarities, however. Several researchers have suggested that a possible explanation for the O-isotopic discrepancies is that the cloud from which the Sun formed was preferentially enriched with material from massive stars, relative to the general ISM (see, e.g., Schramm & Olive 1982; Henkel & Mauersberger 1993; Henkel et al. 1995; Prantzos, Aubert, & Audouze 1996). In such a scenario, the solar system would have atypical elemental and isotopic abundances compared to the average ISM at the time when it formed.

The average Galactic evolution of O-isotopic ratios implied by radio observations of molecular clouds is indicated in Figure 10 by the gray arrow labeled "GCE-II." We note that this trend passes through the Group 3 oxide grain distribution. In fact, if the two Group 3 grains with solar $^{16}O/^{18}O$ ratios are excluded, the average $^{18}O/^{17}O$ ratio for this group is 3.6, which is remarkably similar to the ISM value. This suggests that the sources of some of these grains may have had isotopic compositions more typical of the ISM than the Sun, and the grains may thus be used to trace the average chemical evolution of the Galaxy.

Group 4 presolar oxide grains are enhanced in ^{17}O and ^{18}O, relative to ^{16}O and the solar O-isotopic ratios. As we discussed above in § 4.3.2, the ^{18}O enrichments observed in these four grains may reflect dredge-up of ^{18}O in some AGB stars. However, as can be seen in Figure 10, Group 4 grains lie at the high-metallicity end of the trends expected for Galactic chemical evolution of O-isotopes. If they originated in red giants with higher than solar metallicity, their $^{16}O/^{18}O$ ratios could simply reflect the initial ratios of their parent stars, without the need to invoke dredge-up of ^{18}O in early thermal pulses. The higher than solar $^{25}Mg/^{24}Mg$ and $^{26}Mg/^{24}Mg$ ratios observed in Group 4 grain T22 also fit in well with this idea because these two ratios are also expected to increase in the Galaxy with time (Clayton 1988; Timmes et al. 1995). The primary difficulty with this scenario is the high metallicities needed to explain the data. With the assumption that $^{17}O/^{16}O$ and $^{18}O/^{16}O$ increase linearly with Z, a metallicity about 1.6 times as high as solar is needed to explain the least extreme grain, and $Z \sim 3 \times Z_{\odot}$ is required to explain the lowest observed $^{16}O/^{18}O$ ratio. Moreover, their relatively high $^{16}O/^{17}O$ ratios suggest that these grains originated in low-mass stars ($M < 2\ M_{\odot}$) but it is highly unlikely that very high-Z, low-mass (and therefore old) stars had been present to contribute dust to the protosolar cloud. While we cannot rule out low initial $^{16}O/^{18}O$ ratios in the parent stars of Group 4 grains, we propose as a more likely explanation that dredge-up of ^{18}O occurs in some low-mass AGB stars.

It should be clear from the preceding discussion that isotopic measurements of circumstellar oxide grains provide a new approach to the study of the chemical evolution of the Galaxy. In particular, some grains (Group 3) clearly reflect the O-isotopic trends expected for older (low-mass) stars and may provide clues to the precise dependence of O-isotopic ratios on stellar metallicity. Further progress will require a better theoretical understanding of the nucleosynthetic sources of the oxygen isotopes as well as the Galactic dynamics that lead to a spread in compositions even at a given time and place in the Galaxy. The analysis of many more Group 3 oxide grains is desirable as well, particularly measurements of isotopic ratios of additional elements that could provide independent information about chemical evolution. For example, Huss, Fahey, & Wasserburg (1995b) have proposed that the unusual Mg and Ti isotopic ratios observed in a circumstellar (Group 1) Al_2O_3 grain cannot be explained by nucleosynthetic processes within a single star of initially solar composition but may be understood in terms of Galactic chemical evolution. Similarly, Galactic chemical evolution has been invoked to explained the Si and Ti isotopic compositions of circumstellar SiC grains extracted from primitive meteorites (Gallino et al. 1994; Hoppe et al. 1994a; Timmes & Clayton 1996; Clayton & Timmes 1997).

6. NUMBER OF SOURCES

Even though we have argued that most or all of the presolar oxide grains found in meteorites came from a single *type* of star, namely O-rich red giants, the range of compositions observed in the grains cannot be explained by an origin in a single star. The isotopic characteristics of presolar SiC also seem to require many AGB sources (Alexander 1993; Hoppe et al. 1994a). Uncertainties in iso-

topic ratio measurements and in theoretical predictions of stellar nucleosynthesis make it difficult to determine the precise number of sources involved, but we can make some general estimates. As discussed in § 4.3, the O-isotopic ratios of Group 1 and 3 grains reflect the first dredge-up in red giants. Since most mass loss (and thus grain formation) occurs after the first dredge-up and the surface O-isotopic ratios probably do not change after this point, distinct O-isotopic compositions imply distinct stellar sources. In fact, were it not for measurement uncertainty, the number of sources required to explain these grains would be close to the number of grains in the data set. Taking the significant overlap of error bars of many grains into account, however, we estimate that a minimum of ~ 20 stars are needed to explain the O-isotopic ranges for these two groups. Because this estimate does not take into account the "missed" grains with normal $^{16}O/^{18}O$ ratios but anomalous $^{16}O/^{17}O$ ratios (§ 3.2), the real number of sources is almost certainly higher.

The case for multiple sources of Group 2 oxide grains is less clear cut. Cool bottom processing is expected to occur throughout the AGB phase of the evolution of low-mass stars, gradually increasing the surface $^{16}O/^{18}O$ ratio and decreasing the $^{16}O/^{17}O$ ratio (Wasserburg et al. 1995). Since mass loss and grain formation probably also occur throughout the AGB, most Group 2 grains could have originated in the same AGB star, with grains highly depleted in ^{18}O having formed after those with more moderate ^{18}O depletions. The cluster of four Group 2 grains indicated by an ellipse in Figure 6 deviates from the standard Group 2 trend and probably requires a source distinct from that of the main Group 2 population, however. The type of star that produced the Group 4 grains is not known, and we thus cannot estimate the number of sources need to account for them, although the large errors of two Group 4 grains make an origin in a single star for all four Group 4 grains possible.

To summarize, the isotopic data seem to require a minimum of ~ 25 stars to have contributed Al_2O_3 to the early solar system. Note that this number is comparable to the estimate of Alexander (1993), who used sizes and lifetimes of molecular clouds and birth rates of AGB stars to estimate that 10–100 AGB stars contributed SiC to the solar system. Since O-rich and C-rich AGB stars are present in approximately equal numbers in the solar neighborhood (Jura & Kleinmann 1989), this estimate is probably valid for the AGB sources of O-rich dust as well.

7. ABUNDANCE OF STELLAR OXIDE GRAINS

Previous authors have remarked on the apparent deficit of preserved O-rich dust of stellar origin in meteorites, relative to carbonaceous phases (Hutcheon et al. 1994; Nittler et al. 1994; Huss et al. 1994a). Based on the single grain measurements described in § 3.2, we estimate the abundance of circumstellar Al_2O_3 in Tieschitz to be 0.03 ppm, a factor of ~ 10 lower than our estimate for that of presolar SiC in this meteorite. In fact, a large fraction of the SiC in Tieschitz, but no Al_2O_3, may have been destroyed by mild metamorphism (Huss & Lewis 1994c), and the initial ratio of circumstellar SiC to Al_2O_3 in this meteorite was probably even higher. Hutcheon et al. (1994) have estimated presolar SiC in the Orgueil CI meteorite to be more abundant than presolar Al_2O_3 by a factor of ~ 500, based on the identification of a single Al_2O_3 grain. A similar SiC/Al_2O_3 ratio may hold for the Murchison CM meteorite, based again on one grain (Nittler et al. 1993). Without a better determination of the relative proportions of different types of presolar phases, including Al_2O_3, in different types of meteorites, it is difficult to determine what was the true ratio of presolar SiC to Al_2O_3 in the early solar system. We can, however, estimate the expected SiC/Al_2O_3 ratio in dust from AGB stars, the primary sources of both types of presolar grains in meteorites. With the simple assumptions that all Al goes into Al_2O_3 in O-rich stars while all Si goes into SiC in C-rich stars, the expected SiC/Al_2O_3 mass ratio is equal to $0.8 \times (Si/Al) \times$ (dust from C stars)/(dust from O stars). The mass ratio of dust from C stars to that from O stars is estimated to be 1/3 to 1 (Gehrz 1989; Whittet 1992; Jura & Kleinmann 1989), and if $Si/Al = (Si/Al)_\odot \approx 12$, we obtain an expected presolar SiC/Al_2O_3 ratio of ≈ 3 to 10, lower than the, admittedly poorly known, observed ratios in meteorites. Therefore, there indeed appears to be a paucity of presolar O-rich dust in meteorites. This is somewhat surprising in light of the fact that C-rich dust is expected to be less stable in the oxidizing conditions of the interstellar medium and the early solar system.

Oxygen-rich stardust is probably not preferentially destroyed over C-rich dust, either in space or during sample preparation (Hutcheon et al. 1994). More likely, the low abundance of presolar oxide grains is related to their chemical composition and grain size. Most O-rich dust observed around AGB stars and in the interstellar medium is in the form of silicates, not Al_2O_3. Presolar silicates may or may not be preserved in meteorites. For example, circumstellar and interstellar silicates are believed to have an amorphous structure (see, e.g., Whittet 1992) and perhaps did not survive processing on the parent bodies of meteorites. Indeed, it has been suggested that small, glassy metal-rich objects (GEMs) seen in interplanetary dust particles, but not in meteorites, are interstellar O-rich material that was present in the early solar system (Bradley 1994). Even if presolar silicate dust is present in meteorites, it would have been destroyed by the chemical treatments currently used to isolate circumstellar grains. In a preliminary search, we have used our ion-imaging technique to map the $^{16}O/^{18}O$ ratios of $\sim 30{,}000$ 1 μm silicate grains from nonetched samples of Tieschitz and found none of presolar origin.

A significant fraction of presolar oxide grains might be much finer grained than presolar SiC. The maximum size of grains condensing in a stellar atmosphere depends both on mass-loss rates and on the abundance of available condensable atoms in the gas (Draine & Salpeter 1977; Bernatowicz et al. 1996). Mass-loss rates are expected on theoretical grounds to be higher in C-rich AGB stars, particularly in the late ejection stage when the stars become planetary nebulae and shed $\sim 1\ M_\odot$ in $\leq 10^4$ yr (Renzini 1981). Even at these enhanced mass-loss rates, grain growth calculations do not predict micron-sized grains, and the presence of large presolar C-rich grains from AGB stars led to the suggestion that at least some mass loss occurs in high-density clumps sporadically ejected from the stellar surface (Virag et al. 1992; Bernatowicz et al. 1996). Since micron-sized Al_2O_3 grains from O-rich AGB stars do exist, a similar process might occur also in such stars. In fact, Jura (1996) has reported the discovery of large grains around the O-rich red supergiant IRC +10420. Given, however, the higher average mass-loss rates of carbon stars than O-rich stars, a finer grain size distribution for presolar O-rich dust than for

SiC is not implausible. Zinner & Tang (1988) found ^{17}O enrichments in bulk measurements of thousands of tiny oxide grains in a separate from the Murray CM meteorite. If the median value of $^{16}O/^{17}O = 1300$ observed in circumstellar Al_2O_3 grains is representative, the Zinner & Tang data can be explained by the presence of presolar Al_2O_3 at a level of $\sim 1\%$. Since the separates used for their study contained predominately spinels, but presolar acid-resistant oxide grains are mostly Al_2O_3 this result may indeed indicate a higher fraction of presolar Al_2O_3 at grain sizes $\ll 1$ μm than among 1 μm grains. O-isotopic ratio measurements of purified fine-grained Al_2O_3 separates from primitive meteorites would help shed light on the issue.

The abundance of circumstellar spinel ($MgAl_2O_4$) in meteorites is ~ 50 times lower than that of presolar Al_2O_3. As described in §4.1, spinel is predicted by thermochemical calculations to form from Al_2O_3 200–300 K below the condensation temperature of Al_2O_3 (Lattimer et al. 1978; Sharp & Wasserburg 1995; Lodders & Fegley 1995). The lower abundance of spinel may be due to the smaller temperature range over which spinel is stable compared to that of Al_2O_3 (41 K compared to 240 K for a gas of solar composition and a pressure of 2×10^{-8} atm; Lattimer et al. 1978).

An issue related to the overall underabundance of presolar Al_2O_3 is the failure to find, as yet, oxide grains that condensed in supernova ejecta. SiC, graphite, and Si_3N_4 dust grains that almost certainly originated in Type II supernovae have been found in meteorites (Amari et al. 1992; Nittler et al. 1995a, 1996). As discussed in § 4.4, oxide grains are expected to also form in such explosions since much more O than C is ejected and comparison of theoretical calculations with observations of SN 1987A suggests that O-rich dust, including Al_2O_3, formed in this supernova (Kozasa et al. 1991; Colgan et al. 1994). If all Al in O-rich supernova shells goes into Al_2O_3 and all Si in C-rich shells goes into SiC, the calculated supernova yields of Woosley & Weaver (1995) give Al_2O_3/SiC ratios of ~ 4–20 by mass in the ejecta of stars of mass 15–25 $M_\odot$. If we combine these ratios with our above estimate of 3–10 for the SiC/Al_2O_3 ratio in dust from AGB stars, and with the observed ratio of presolar meteoritic SiC from supernovae to that from AGB stars, 1% (Amari et al. 1992; Nittler et al. 1995a), we estimate that the ratio of presolar Al_2O_3 from supernovae to that from AGB stars should be at least 0.1–2. This estimate is in sharp contrast to the upper limit of a few percent observed in the current presolar oxide grain data set. Grain size may again play a role. Kozasa et al. (1991) have suggested that the infrared light curve observed in SN 1987A is due to very small (10 Å) Al_2O_3 grains condensing in the ejecta.

Regardless of theoretical expectations of SN dust production, the presence of presolar oxide grains from supernovae has been suggested for more than 20 years to explain endemic ^{16}O enrichments in the most refractory solar system phases in meteorites (Clayton et al. 1973; Clayton 1977; Clayton 1993). However, our data show no evidence for ^{16}O-rich presolar oxide grains in the solar nebula. The discovery of chemical processes that result in mass-independent fractionation of O-isotopes (Thiemens & Heidenreich 1983) removes the requirement that ^{16}O excesses in meteorites are nucleosynthetic in origin but a connection between such processes and processes in the early solar system has yet to be proven.

8. SUMMARY AND CONCLUSIONS

We have presented O- and Al-Mg isotopic data for 46 new and 42 previously reported stellar oxide grains (86 Al_2O_3 and two $MgAl_2O_4$) identified in separates of primitive meteorites. The isotopic data are classified into four distinct groups. An additional group of grains may be represented by a single member, the extremely ^{17}O-enriched grain T54. The data were discussed in the context of astronomical observations and theoretical models of stellar evolution, nucleosynthesis, and Galactic chemical evolution. Our primary conclusions can be summarized as follows:

1. Most or all of the grains probably formed in stellar winds from low to intermediate mass red giants and AGB stars. However, the compositions of the different groups of grains reflect different astrophysical processes occurring in the parent stars and provide new information about these processes.

Group 1 grains have O-isotopic compositions consistent with the results of calculations of the first dredge-up that occurs in red giants at the end of core H burning. Many also have ^{26}Mg excesses, with inferred $^{26}Al/^{27}Al$ ratios in the range predicted for third dredge-up in AGB stars. Grains without evidence for ^{26}Al probably formed before the AGB phase of evolution, even though the high mass-loss rates needed to grow micron-sized grains are thought not to occur until the AGB. Furthermore, the similarity of the O-isotopic ratios of Group 1 grains with and without ^{26}Al indicates that the third dredge-up does not appreciably change the surface O-isotopic ratios of most O-rich AGB stars.

The O-isotopic ratios of *Group 2* grains are most plausibly explained by "extra mixing" of material at the base of the convective envelope to the hotter regions near the H-burning shell in AGB stars ("cool bottom processing"; Wasserburg et al. 1995), although realistic mixing models are needed to test this hypothesis. Comparing grain data with parameterized calculations (Wasserburg et al. 1995), we estimate that cool bottom processing sufficient to destroy ^{18}O in AGB stars occurs only in stars of mass $\lesssim 1.5$ $M_\odot$.

Group 3, like Group 1, grains have O-isotopic ratios that appear to reflect first dredge-up in red giant stars. However, their high ($\gtrsim$solar) $^{16}O/^{17}O$ ratios imply that they originated in very low-mass (1.2–1.4 $M_\odot$) stars. Furthermore, the stellar sources of these grains must have had initial $^{16}O/^{17}O$ and $^{16}O/^{18}O$ ratios higher than the solar values. The presence of excess ^{26}Mg in only a small fraction of these grains is consistent with theoretical predictions that, in very low-mass stars, most mass loss occurs before the AGB phase and its third dredge-up (Boothroyd & Sackmann 1988).

Group 4 grains have large ^{18}O enrichments, relative to solar. The $^{16}O/^{17}O$ ratios and Mg-isotopic compositions of these grains are consistent with an origin in low-mass AGB stars, but the origin of the excess ^{18}O is unknown. Possible explanations are that ^{18}O, produced by α captures on ^{14}N in early thermal pulses, is dredged up in some stars before it is converted to ^{22}Ne or that the grains come from high-metallicity stars whose initial ^{18}O abundance was high. Although the data do not allow us to distinguish between these two explanations, we consider the latter possibility to be unlikely since it would require low-mass stars with metallicity much higher than that of the Sun to have ended

their lives at the time the solar system formed. However, the possibility of dredge-up of ^{18}O in some AGB stars needs to be confirmed by detailed stellar models.

Grain T54 has a substantial ^{18}O depletion and an $^{17}O/^{16}O$ ratio 37 times that of the solar value. If the $^{16}O/^{18}O$ ratio of this grain is the measured value, we are unaware of any stellar source that could produce its composition. If, however, the ^{18}O measured in this grain came from the supporting sample mount (a distinct possibility), T54 has the O-isotopic composition expected of hot bottom burning in relatively high-mass (> 4–$5\ M_{\odot}$) AGB stars or of the surface of massive mass-losing stars (Wolf-Rayet) in the Of-WN stages of evolution. Additional data on grains of this type may help distinguish between these possibilities.

2. The presolar oxide grains require at least 25 distinct AGB sources, consistent with estimates of the number of such stars that provided dust to the solar system (Alexander 1993). Note that the true number of sources is higher, since many Group 1 grains have no doubt been missed in the ion-imaging searches used to find most of the grains.

3. Galactic chemical evolution plays a recognizable role in determining the isotopic compositions of many circumstellar oxide grains. In particular, the higher than solar $^{16}O/^{17}O$ and $^{16}O/^{18}O$ ratios of Group 3 grains indicate that they come from low-mass red giants formed early in the Galaxy when the interstellar medium was, on average, less enriched in the secondary isotopes ^{17}O and ^{18}O, relative to the primary isotope ^{16}O. The range of $^{16}O/^{18}O$ ratios of grains in Groups 1 and 3 is consistent with observations that indicate a wide spread in metallicity for stars that form at a given time and place in the Galaxy (Edvardsson et al. 1993).

4. Possible explanations for the apparent underabundance of presolar O-rich dust in meteorites relative to presolar carbonaceous phases are (1) most O-rich stardust is in the form of acid-soluble silicates, not acid-resistant oxides such as Al_2O_3 and $MgAl_2O_4$, and is thus destroyed in the treatments used to enrich presolar grains; and (2) relative mass-loss rates of O-rich AGB stars and carbon stars suggest that O-rich dust has a finer grain size distribution than C-rich dust and may therefore go undetected in our ion probe studies. The lack of oxide grains from supernovae is surprising; it may also be related to grain size.

This work demonstrates that stellar oxide dust grains in meteorites, although difficult to locate, are a new source of information, complementary to astronomical observations, for a better understanding of diverse astrophysical processes, from stellar nucleosynthesis and mixing to the chemical evolution of the Galaxy.

We thank T. Bernatowicz, A. Boothroyd, D. D. Clayton, R. Cowsik, M. F. El Eid, R. Gallino, and S. Woosley for many helpful discussions. We are especially grateful to A. Boothroyd, F. Timmes, and S. Woosley for sharing the results of their calculations in computer-readable form. We acknowledge P. Hoppe's initial role in developing the ion-imaging technique. This work was funded by NASA grant NAGW 3371.

REFERENCES

Aitken, D. K., Roche, P. F., Spenser, P. M., & Jones, B. 1979, ApJ, 233, 925
Alexander, C. M. O'D. 1993, Geochim. Cosmochim. Acta, 57, 2869
Amari, S., Anders, E., Virag, A., & Zinner, E. 1990, Nature 345, 238
Amari, S., Hoppe, P., Zinner, E., & Lewis, R. S. 1992, ApJ, 394, L43
———. 1995a, Meteoritics, 30, 679
Amari, S., Lewis, R. S., & Anders, E. 1994, Geochim. Cosmochim. Acta, 58, 459
———. 1995b, Geochim. Cosmochim. Acta, 53, 1411
Anders, E., & Zinner, E. 1993, Meteoritics, 28, 490
Bernatowicz, T. J., Amari, S., & Lewis, R. S. 1992, Lunar Planet. Sci., 23, 91
Bernatowicz, T. J., Amari, S., Zinner, E. K., & Lewis, R. S. 1991, ApJ, 373, L73
Bernatowicz, T. J., Cowsik, R., Gibbons, P. C., Lodders, K., Fegley, B., Jr., Amari, S., & Lewis, R. S. 1996, ApJ, 472, 760
Bernatowicz, T., Fraundorf, G., Tang, M., Anders, E., Wopenka, B., Zinner, E., & Fraundorf, P. 1987, Nature 330, 728
Blackmon, J. C., Champagne, A. E., Hofstee, M. A., Smith, M. S., Downing, R. G., & Lamaze, G. P. 1995, Phys. Rev. Lett., 74(14), 2642
Bode, M. F., Evans, A., Whittet, D. C. B., Aitken, D. K., Roche, P. F., & Whitmore, B. 1984, MNRAS, 207, 897
Boothroyd, A. I. & Sackmann, I.-J. 1988, ApJ, 328, 653
———. 1997, ApJ, submitted
Boothroyd, A. I., Sackmann, I.-J., & Wasserburg, G. J. 1994, ApJ, 430, L77
———. 1995, ApJ, 442, L21
Bradley, J. P. 1994, Science, 265, 925
Bressan, A., Fagotto, F., Bertelli, G., & Chiose, C. 1993, A&AS, 100, 647
Cameron, A. G. W. 1993, in Protostars and Planets III, ed. E. H. Levy & J. Lunine (Tucson: Univ. of Arizona Press), 47
Cameron, A. G. W., & Fowler, W. A. 1971, ApJ, 164, 111
Catanzaro, E. J., Murphy, T. J., Garner, E. L., & Shields, W. R. 1966, J. Res. NBS, 70a, 453
Charbonnel, C. 1994, A&A, 282, 811
———. 1995, ApJ, 453, L41
Clayton, D. D. 1977, Icarus, 32, 255
———. 1983, Principles of Stellar Evolution and Nucleosynthesis (New York: McGraw-Hill)
———. 1988, ApJ, 334, 191
Clayton, D. D., & Timmes, F. X. 1997, ApJ, 483, 220
Clayton, R. N. 1993, Ann. Rev. Earth Planet. Sci., 21, 115
Clayton, R. N., Grossman, L., & Mayeda, T. K. 1973, Science, 182, 485
Colgan, S. W. J., Haas, M. R., Frickson, E. F., & Lord, S. D. 1994, ApJ, 427, 874
Dearborn, D. S. P. 1992, Phys. Rep., 210, 367
Draine, B., & Salpeter, E. 1977, J. Chem. Phys., 67, 2230
Edvardsson, B., Anderson, J., Gustaffson, B., Lambert, D. L., Nissen, P. E., & Tomkin, J. 1993, A&A, 275, 101
El Eid, M. 1994, A&A, 285, 915
Fahey, A. J., Goswami, J. N., McKeegan, K. D., & Zinner, E. 1987, Geochim. Cosmochim. Acta, 51, 329
Forestini, M., Paulus, G., & Arnould, M. 1991, A&A, 252, 597
Frost, C. A., & Lattanzio, J. C. 1996, in Proc. 32d Liège Internat. Astrophys. Colloq., ed. A. Noels, D. Fraipont-Caro, M. Gabriel, N. Grevesse, & P. Demarque (Liège: Université de Liège), 307
Gallino, R., Raiteri, C. M., Busso, M., & Matteucci, F. 1994, ApJ, 430, 858
Gehrz, R. D. 1988, ARA&A, 26, 377
———. 1989, in Interstellar Dust, ed. L. J. Allamandola & A. G. G. Tielens (Dordrecht: Kluwer), 445
Gehrz, R. D., Grasdalen, G. L., Greenhouse, M., Hackwell, J. A., Heyward, T., & Bentley, A. F. 1986, ApJ, 281, 303
Gilroy, K. K. 1989, ApJ, 347, 835
Gilroy, K. K., & Brown, J. A. 1991, ApJ, 371, 578
Guélin, M., Forestini, M., Valiron, P., Ziurys, L. M., Anderson, M. A., Cernicharo, J., & Kahane, C. 1995, A&A, 297, 183
Gustafsson, B. 1989, AR&A, 27, 701
Harris, M. J., & Lambert, D. L. 1984a, ApJ, 281, 739
———. 1984b, ApJ, 285, 674
Harris, M. J., Lambert, D. L., Hinkle, K. H., Gustafsson, B., & Eriksson, K. 1987, ApJ, 316, 294
Harris, M. J., Lambert, D. L., & Smith, V. V. 1985, ApJ, 292, 620
———. 1988, ApJ, 325, 768
Henkel, C., & Mauersberger, R. 1993, A&A, 274, 730
Henkel, C., Wilson, T. L., Langer, N., Chin, Y.-N., & Mauersberger, R. 1995, in The Structure and Content of Molecular Clouds, ed. T. L. Wilson & K. J. Johnston (Berlin: Springer), 72
Herant, M., & Woosley, S. E. 1994, ApJ, 425, 814
Hoppe, P., Amari, S., Zinner, E., Ireland, T., & Lewis, R. S. 1994a, ApJ, 430, 870
Hoppe, P., Strebel, R., Eberhardt, P., Amari, S., & Lewis, R. S. 1994b, Lunar Planet. Sci., 25, 563
Hunter, J. L., Jr., Linton, R., & Griffis, D. P. 1991, J. Vacuum Sci. Technol. A, 9(3), 1622
Huss, G. R., Fahey, A. J., Gallino, R., & Wasserburg, G. J. 1994a, ApJ, 430, L81
Huss, G. R., Fahey, A. J., & Wasserburg, G. J. 1994b, Meteoritics 29, 475

Huss, G. R., Fahey, A. J., & Wasserburg, G. J. 1995a, Lunar Planet. Sci., 26, 645
———. 1995b, Lunar Planet. Sci., 26, 643
Huss, G. R., Hutcheon, I. D., Wasserburg, G. J., & Stone, J. 1992, Lunar Planet. Sci., 23, 563
Huss, G. R., & Lewis, R. S. 1994a, Meteoritics 29, 791
———. 1994b, Meteoritics 29, 811
———. 1994c, Geochim. Cosmochim. Acta, 59, 115
Hutcheon, I. D., Huss, G. R., Fahey, A. J., & Wasserburg, G. J. 1994, ApJ, 425, L97
Iben, I., Jr. 1967, ARA&A, 5, 571
Iben, I., Jr., & Renzini, A. 1983, ARA&A, 21, 271
Jura, M. 1996, ApJ, 472, 806
Jura, M., & Kleinmann, S. G. 1989, ApJ, 341, 359
Kahane, C., Cernicharo, J., Gomez-Gonzalez, J., & Guélin, M. 1992, A&A, 256, 235
Kozasa, T., Hasegawa, H., & Nomoto, K. 1991, A&A, 474
Kwok, S., & Chan, S. J. 1993, AJ, 106(5), 2140
Lambert, D. L. 1991, in Evolution of Stars: The Photospheric Abundance Connection, ed. G. Michaud & A. Tutukov (Dordrecht: Kluwer), 299
Landré, V., Prantzos, N., Auger, P., Bogaert, G., Lefebvre, A., & Thibaud, J. P. 1990, A&A, 240, 85
Lattimer, J. M., Schramm, D. N., & Grossman, L. 1978, ApJ, 219, 230
Lewis, R. S., Amari, S., & Anders, E. 1994, Geochim. Cosmochim. Acta, 58, 471
Lewis, R. S., Tang, M., Wacker, J. F., Anders, E., & Steel, E. 1987, Nature 326, 160
Little-Marenin, I. R. 1986, ApJ, 307, L15
Lodders, K., & Fegley, B., Jr. 1995, Meteoritics, 30, 661
MacPherson, G. J., Davis, A. M., & Zinner, E. K. 1995, Meteoritics, 30, 365
Mathews, G. J., Bazan, G., & Cowan, J. J. 1992, ApJ, 391, 719
McKeegan, K. D. 1987, Science, 237, 1468
McKeegan, K. D., Walker, R. M., & Zinner, E. 1985, Geochim. Cosmochim. Acta, 49, 1971
Mowlavi, N. 1995, Ph.D. thesis, Université Libre de Bruxelles
Nichols, R. H., Jr., Hohenberg, C. M., Amari, S., & Lewis, R. 1991, Meteoritics, 26, 377
Nichols, R. H., Jr., Kehm, K., Brazzle, R., Amari, S., Hohenberg, C. M., & Lewis, R. S. 1994, Meteoritics, 29, 510
Nittler, L. R. 1996, Lunar Planet. Sci., 27, 965
Nittler, L. R., Alexander, C. M. O'D., Gao, X., Walker, R. M., & Zinner, E. K. 1994, Nature, 370, 443
———. 1995a, in Nuclei in the Cosmos III, ed. M. Busso, R. Gallino, & C. M. Raiteri (New York: AIP), 585
Nittler, L. R., Amari, S., Zinner, E., Woosley, S. E., & Lewis, R. S. 1996, ApJ, 462, L31
Nittler, L. R., & Cowsik, R. 1997, Phys. Rev. Lett., 78(2), 175
Nittler, L. R., et al. 1995b, ApJ, 453, L25
Nittler, L. R., Walker, R. M., Zinner, E., Hoppe, P., & Lewis, R. S. 1993, Lunar Planet. Sci., 24, 1087
Nørgaard, H. 1980, ApJ, 236, 895
Onaka, T., De Jong, T., & Willems, F. J. 1989, A&A, 218, 1690
Ott, U. 1993, Nature 364, 25
Penzias, A. A. 1981, ApJ, 249, 518
Politano, M., Starrfield, S., Truran, J. W., Weiss, A., & Sparks, W. M. 1995, ApJ, 448, 807
Prantzos, N., Aubert, O., & Audouze, J. 1996, A&A, 309, 760
Prantzos, N., Doom, C., Arnould, M., & de Loore, C. 1986, ApJ, 304, 695
Renzini, A. 1981, in Physical Processes in Red Giants, ed. I. Iben, Jr. & A. Renzini (Dordrecht: Reidel), 431
Rolfs, C. E., & Rodney, W. S. 1988, Cauldrons in the Cosmos (Chicago: Univ. of Chicago Press)
Schaller, G., Schaerer, D., Meynet, G., & Maeder, A. 1992, A&AS, 96, 269
Schramm, D. N., & Olive, K. A. 1982, Ann. NY Acad. Sci., 395, 236
Sharp, C. M., & Wasserburg, G. J. 1995, Geochim. Cosmochim. Acta, 59, 1633
Shigeyama, T., & Nomoto, K. 1990, ApJ, 360, 242
Smith, V. V., & Lambert, D. L. 1990, ApJS, 72, 387
Sugimoto, D. 1971, Prog. Theoret. Phys. 45, 761
Tang, M., & Anders, E. 1988, Geochim. Cosmochim. Acta, 52, 1235
Thielemann, F. K., Nomoto, K., & Yokoi, K. 1986, A&A, 158, 17
Thiemens, M. H., & Heidenreich, J. E. 1983, Science 219, 1073
Timmes, F. X., & Clayton, D. D. 1996, ApJ, 472, 723
Timmes, F. X., Woosley, S. E., & Weaver, T. A. 1995, ApJ, 98, 617
Treffers, R., & Cohen, M. 1974, ApJ, 188, 545
Virag, A., Wopenka, B., Amari, S., Zinner, E., Anders, E., & Lewis, R. S. 1992, Geochim. Cosmochim. Acta, 56, 1715
Virag, A., Zinner, E., Amari, S., & Anders, E. 1991, Geochim. Cosmochim. Acta, 55, 2045
Wasserburg, G. J., Boothroyd, A. I., & Sackmann, I.-J. 1995, ApJ, 447, L37
Wasserburg, G. J., Busso, M., Gallino, R., & Raiteri, C. M. 1994, ApJ, 424, 412
Whittet, D. C. B. 1992, Dust in the Galactic Environment (New York: Institute of Physics)
Wiescher, M., Giesen, U., Görres, J., Azuna, R. E., Kratz, K. L., & Trautvetter, H.-P. 1993, in Nuclei in the Cosmos, ed. F. Käppeler & K. Wisshak (New York: IOP), 191
Willems, F. J., & De Jong, T. 1986, ApJ, 309, L39
Wilson, T. L., & Rood, R. T. 1994, AR&A, 32, 191
Woosley, S. E. 1986, in Nucleosynthesis and Chemical Evolution, ed. B. Hauck, G. Maeder, & G. Meynet (Geneva: Observatoire de Genève), 1
Woosley, S. E., & Weaver, T. A. 1995, ApJS, 101, 181
Zahn, J. P. 1992, A&A, 265, 115
Zinner, E., & Tang, M. 1988, Lunar Planet. Sci., 19, 1323

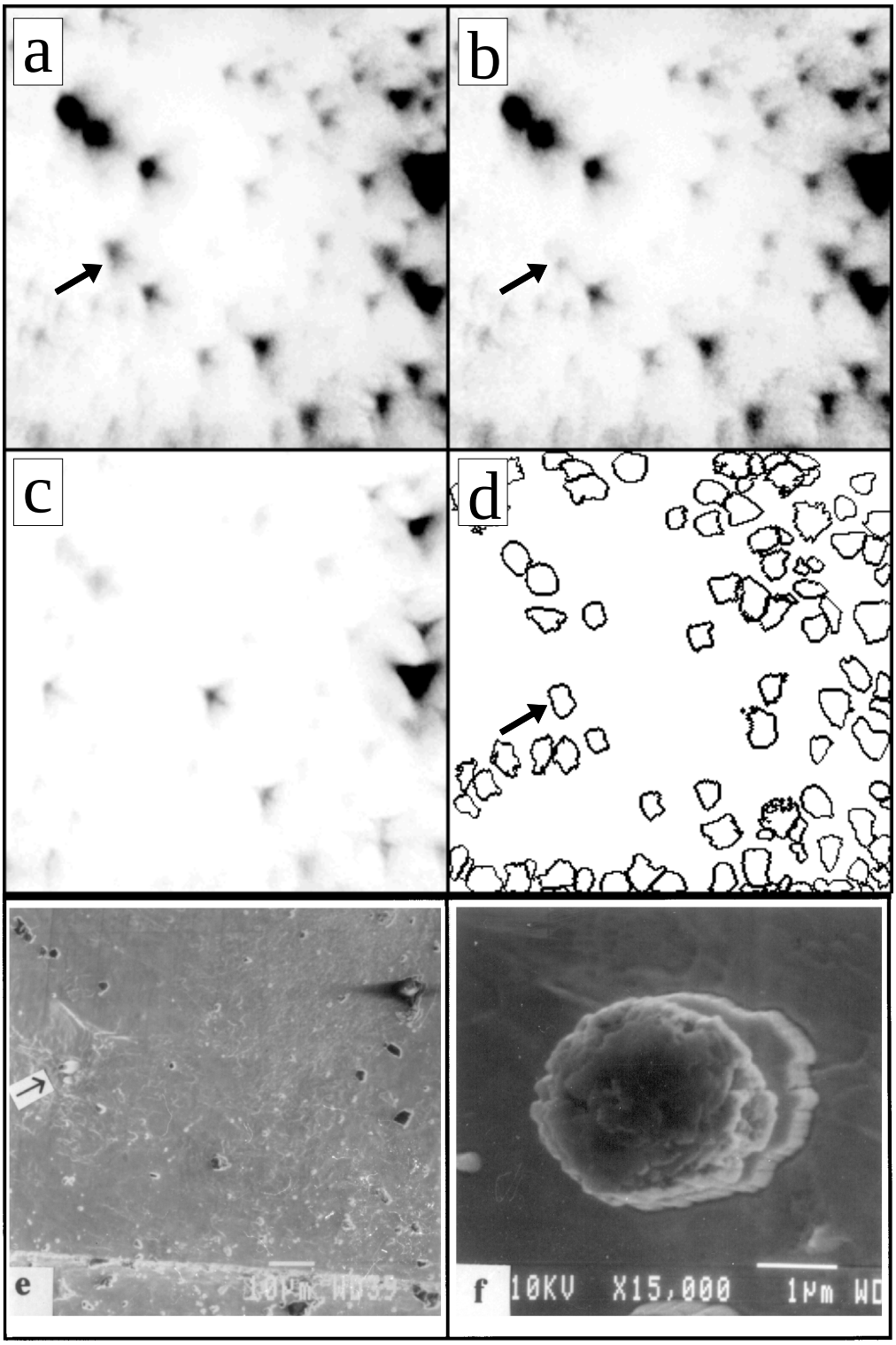

FIG. 1.—Sample ion images of a 100 μm × 100 μm area of a sample mount containing grains extracted from the Tieschitz meteorite. Images are (*a*) ^{16}O, (*b*) ^{18}O, (*c*) ^{28}Si, (*d*) contours showing results of automatic particle definition in oxygen images, (*e*) SEM micrograph of same area, and (*f*) high-magnification micrograph of isotopically anomalous presolar Al_2O_3 grain indicated by arrow in (*a*), (*b*), and (*d*).

NITTLER et al. (see 483, 477)